

DISSERTATION

Combining Eddy-Current and Micromagnetic Simulations with Finite-Element method

ausgeführt zum Zwecke der Erlangung des akademischen Grades eines Doktors der
technischen Wissenschaften unter der Leitung von

Univ.Prof. Dipl.-Ing. Dr.techn. Thomas Schrefl

E138

Institut für Festkörperphysik

eingereicht an der Technischen Universität Wien

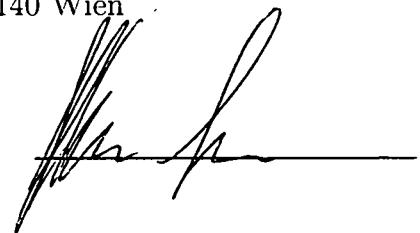
Fakultät für Physik von

Dipl.-Ing. Gino Hrkac

Matr.Nr. 9526355

Linzerstrasse 160/1/7, 1140 Wien

Wien, am 15. September 2005



Contents

Abstract	5
Kurzfassung	7
Acknowledgment	9
1 Introduction	11
2 Finite Element and Boundary Element Method	14
2.1 Poisson and Laplace Problem	15
2.2 The Weak Formulation	16
2.3 The Galerkin Discretization	16
2.4 Boundary Element Method	18
2.5 Mesh Generation	20
3 Principles of Magnetization Motion	24
3.1 Quantum-Mechanical Concepts	25
3.2 Lagrangian Formulation of the Equation of Motion	29
3.2.1 Lagrangian formulation	29
3.2.2 Landau–Lifshitz–Gilbert Equation	31
4 Micromagnetics	33

	3
4.1 Basic Principles of Micromagnetics	35
4.2 Total magnetic Gibbs free Energy	35
4.2.1 Anisotropy Energy	36
4.2.2 Exchange Energy	39
4.2.3 Magnetostatic Field	41
4.3 Browns Equations	42
5 Micromagnetics and LLG Equation	45
6 Eddy Currents	48
6.1 Eddy Current Model	50
6.1.1 Eddy Current Diffusion Equation	50
6.1.2 Boundary Conditions	54
6.2 Calculation of the Eddy Current Field	56
7 Numerical Technique and Algorithm	59
7.1 Implicit Differential Algebraic Solver	60
7.1.1 Error control	62
8 Eddy Current and Magnetization	64
8.1 Finite Element Discretization	65
8.2 Precession and Damping Term	67
8.2.1 Magnetization Reversal	70
8.3 Precession and Damping Term including Eddy Currents	74
8.4 Demagnetization Field and Eddy Currents	78
8.5 Conclusions	80
9 Eddy Currents in Sub-Micron Permalloy Structures	81
9.1 Diffusion Equation and Material Parameters	82

	4
9.2 Eddy Currents and Material Parameters	83
9.3 The Eddy Current Diffusion Parameter	86
9.4 Eddy currents and Critical Size of Single Domain Behavior	89
9.5 Conclusions	97
10 Influence of Eddy currents on the Effective Damping Parameter	98
10.1 Model	99
10.2 Eddy Currents and the Effective Damping Parameter	100
10.3 Permalloy Single Particle Simulations	102
10.4 Conclusions	105
List of Figures	107
Bibliography	111
Curriculum vitae	118
Lebenslauf	119
List of Publications	120

Abstract

Eddy current effects are usually not taken into account in micro magnetic simulations of magnetization reversal of magnetic nano-structures. The net contribution of eddy currents is assumed to be already included in the damping parameter of the Landau-Lifshitz-Gilbert equation (LLG). The increasing demand of ultra-fast switching in magnetic nanostructures demands a more accurate model for high-speed switching in conducting ferromagnetic materials. It is apparent that eddy currents which are induced by high frequency fields with rise times of < 0.1 ns affect the magnetization behavior of the conducting ferromagnetic materials.

In this work a micromagnetic eddy current method was developed that allows arbitrary geometries, requires no mesh outside the ferromagnetic particles, and uses a stable integration scheme. It simultaneously solves the Landau-Lifshitz-Gilbert equation and the quasi-static Maxwell equations using a hybrid finite element/boundary element method (FEM/BEM). The eddy current field is introduced as part of the total effective field and is directly calculated from the space time behavior of the magnetization rate of change. The boundary conditions of the eddy current field at infinity are taken into account using a FEM/BEM scheme. The resulting system of differential algebraic equations is solved using a backward differentiation method.

From the derived eddy current diffusion equation the critical particle size and conductivity range that leads to pronounced eddy current effects on magnetization reversal of magnetic nano-structures is determined.

It is shown that the size of the particles, which designates the coherence of the spin structure, is essential for the eddy current net contribution to the effective damping parameter, which is a function of particle size and electric conductivity, and directly influences the magnetization reversal process in sub-micron permalloy structures.

Recapitulating: In this thesis a theory that explains eddy current effects in single and multi-domain particles was developed. Based on the theory a model was derived that predicts eddy current contributions in multi-scale particles, which allows to design and predict the behavior of materials that will be used in future magnetic recording heads as well as in magnetic data storage medias.

Kurzfassung

In herkömmlichen mikromagnetischen Simulationen von Ummagnetisierungsprozessen magnetischer Nanopartikeln werden Wirbelströme nicht berücksichtigt. Der Wirbelstrombeitrag wird als ein Teil des Dämpfungsparameters der Landau-Lifshitz-Gilbert Gleichung betrachtet. Der steigende Bedarf an ultraschnellem Schaltverhalten in leitenden Ferromagneten macht genauere Modelle für das Ummagnetisierungsverhalten von magnetischen Nanopartikeln notwendig.

In dieser Arbeit wird ein mikromagnetisches Wirbelstrom-Modell basierend auf einer Finite-Element Methode vorgestellt, das das Modellieren von allgemeinen Strukturen erlaubt, kein Finite-Element Gitter für den Aussenraum benötigt und ein stabiles Integrationschema verwendet. Dieses Modell löst die Landau-Lifshitz-Gilbert Gleichung und die Maxwell-Gleichungen gleichzeitig in einer quasistatischen Näherung mit einer kombinierten Finite Element/Boundary Element Methode. Hierbei werden die Wirbelströme als Teil des totalen effektiven Feldes in das Gleichungssystem integriert und direkt aus dem zeitlichen Verhalten der Magnetisierungsänderung berechnet. Die Randbedingungen im Unendlichen werden durch ein Randintegralschema berechnet. Das resultierende System von Algebraischen und Differentialgleichungen wird mit einer Backward Differentiation Methode gelöst. Die Diffusionsgleichung für Wirbelströme wurde abgeleitet und daraus die kritische Partikelgröße sowie die Leitfähigkeit bestimmt, die notwendig sind, damit die Wirbelströme einen essentiellen Beitrag zum Magnetisierungsprozess von magnetischen Nanopartikeln leisten.

Es wird gezeigt, dass die Partikelgröße, die der bestimmende Faktor für die Koherenz der Spinstruktur ist, den Beitrag der Wirbelströme zum effektiven Dämpfungsparameter bestimmt. Desweiteren wird gezeigt, dass der Dämpfungsparameter eine Funktion der Partikelgröße und der elektrischen Leitfähigkeit ist und einen direkten Einfluß auf das Ummagnetisierungsverhalten von Submikrostrukturen hat.

Zusammenfassend wurde in der vorliegenden Arbeit eine Theorie entwickelt, die den Effekt von Wirbelströmen in Partikeln mit einer oder mehreren Domänen beschreibt. Von dieser Theorie ausgehend wurde ein Modell hergeleitet, das den Beitrag von Wirbelströmen in Partikeln über mehrere Größenskalen vorhersagt. Das ermöglicht es, das Verhalten von Materialien vorherzusagen und Materialien mit erwünschten Eigenschaften zu entwickeln, die in zukünftigen magnetischen Schreibleseköpfen als auch in magnetischen Speichermedien zum Einsatz kommen können.

Acknowledgment

"Die vernünftigen Menschen passen sich der Welt an; die unvernünftigen versuchen, sie zu verändern. Deshalb hängt aller Fortschritt von den Unvernünftigen ab."

"The reasonable man adapts himself to the world. The unreasonable man persists in trying to adapt the world to himself. Therefore, all progress depends on the unreasonable man."

G. B. Shaw

I would like to thank Thomas Schrefl for giving me the opportunity to work on exciting and challenging topics. His support, advice and encouraging words helped me a lot when sometimes things did not evolve as they should. With his enthusiasm and his special view of the world he showed, that almost everything can be done. I would also like to thank him for the opportunity to attend many conferences and to visit other research groups all around the world, especially the unforgettable time I spend in Sheffield. This gave me the chance to work with many interesting people and to exchange scientific knowledge.

I want to thank my colleagues Hermann Forster, Otmar Ertl, Markus Kirschner, Florian Dorfbauer, Jehyun Lee and Dieter Suess for a great time during work, on conferences but also for activities beyond physics. Hermann, thank you for the first

and warm welcome you gave me when I joined the group. A special thank to Florian and Markus for their technical support. Florians knowledge really saved me a lot of time with all computer related problems. Otmar, I want to thank for the scientific discussions and the after work activities. The collaborations with my colleagues led to many joint publications and participations on conferences.

Special thanks to Josef Fidler for creating a lively group of young and enthusiastic physicists which made a very good working atmosphere.

The research visit at the Hitachi San Jose Research Center was an unforgettable experience for me. For that many thanks to Manfred Schabes who invited me.

Veronika, there are many things I should be thankful for. Your patience and your soothing words for the times when things did not turn out as they should. You were there for me when times have grown to be difficult. Thank you for all your support!

At last I want to thank my family and especially my father who encouraged me to follow my dreams and to be true to myself.

Finally, I want to acknowledge the financial support of the Austrian Science Fund, Y-132 PHY.

Chapter 1

Introduction

The main motivation to develop a dynamic micromagnetic model that includes eddy currents is the importance of accurate calculations of time dependent micromagnetic processes for magnetic data storage (hard disk recording, magnetic random access memory MRAM) at high data rates and the demand for ultra-fast switching in magnetic nanostructures, that comprise submicron elements of ferromagnetic material, usually Permalloy. Computational micromagnetics presents an efficient tool to study these kind of ultra fast spin dynamics.

The notion of spin and spin-dynamic was introduced by the conceptual breakthrough offered by quantum mechanics. In the 1935 paper of Landau and Lifshitz [16] and in the 1956 paper of Gilbert [6] a complementary view to spin motion based on the interaction between conservative precession around the spins effective field and a dissipative damping associated with this movement was introduced. Kikuchi [53] was the first who investigated the minimum switching time when magnetization motion is essentially governed by precession. The influence of dissipative damping was taken care of by the introduction of a so called damping term which is mainly governed by a damping constant.

Eddy currents are usually not taken into account in micro magnetic simulations of

magnetization reversal of magnetic nano-structures. The net contribution of eddy currents is assumed to be already included in the damping parameter of the Landau-Lifshitz-Gilbert equation of motion. These kind of assumptions are no longer applicable for magnetic particles in magnetic fields with field rise times of less than 0.1 ns and a conductivity σ of more than $1.10^6 (\Omega\text{m})^{-1}$.

Several models and methods were presented in the past to analyze the influence of eddy current effects on magnetization dynamics. These include the two-dimensional quasi-static model by Della Torre and Eicke [39] and the one-dimensional dynamic calculations by Sandler and Bertram [40]. Mayergoyz et al [50] presented a self-consistent numerical solution of the magnetic diffusion equation and the Landau-Lifshitz equation and showed the effect of eddy currents for different conducting materials.

In this work a three-dimensional finite element dynamic micromagnetic model including eddy currents was developed. The model simultaneously solves the Landau-Lifshitz-Gilbert (LLG) equation and the quasi static Maxwell equation using a hybrid FE/BE method. A finite element method with a linear basis function is used to discretize the conducting region Ω . To calculate the magnetization vector on each node of our mesh an additional discretization, the delaunay-voronoi discretization, was used to calculate the exact volume around each node, which proved to be more accurate than the mass-lumping method that had been used before. The boundary element method is used to map the boundary conditions of the magnetic field at infinity on equivalent boundary conditions on the surface of the conducting region Ω , which reduces the necessity of a mesh to Ω , allowing arbitrary geometries. The FEM/BEM method is described in detail in chapter 2. The magnetization dynamics are governed by the Landau-Lifshitz-Gilbert equation of motion, which is derived out of the principles of magnetization motion, starting from quantum mechanical concepts and lagrangian formulation, found in chapter 3, and the basic magnetic principles summarized in chapter 4. The eddy current field is introduced as an additional part

of the effective magnetic field in the Landau–Lifshitz–Gilbert (LLG) equation and is directly calculated from the space time behavior of the magnetization rate of change. The derivation of the eddy current field is explained in chapter 6, and the numerical techniques are described in chapter 7.

Chapter 8 explains the theory of eddy current effects on the precession and damping term of the LLG equation. The model is used to investigate the impact of eddy currents on the magnetization behavior of materials with different conductivity and size, the results and conclusions are given in chapter 9. Finally, in chapter 10, a method for the calculation of the effective damping parameter as a function of particle size and electric conductivity is presented and used to extract the eddy current contribution from the effective damping constant.

Chapter 2

Finite Element and Boundary Element Method

The hybrid FEM/BEM approach retains the advantages of both, differential equation and integral equation approaches. The general procedure for a hybrid technique requires that the region of interest be enclosed by an artificial boundary. Maxwells equations are then solved by a differential equation approach such as the finite element method (FEM) inside the artificial boundary and by an integral equation approach in discretized form such as the boundary element method (BEM) outside the artificial boundary. Although use of BEM on and outside the artificial boundary results in a full dense matrix, convergence of an approximate solution to the exact solution is guaranteed without a change in the location of the artificial boundary. This method will be introduced in detail for the solution of the Poisson and the Laplace equation, as the former are used in the following chapters to solve the micromagnetic equations.

2.1 Poisson and Laplace Problem

The aim is to find a solution U , that approximates the exact solution u of the Poisson and Laplace equation which are both elliptic partial differential equations. In 3 dimensions, the problem is to find a twice-differentiable real-valued function u of real valued variables x, y, z in a region Ω in \mathbb{R}^3 with a closed boundary Γ .

In the following $H^1(\Omega)$ belongs to the Sobolev spaces and $L^2(\Omega)$ is the space of square integrable functions on the (bounded) domain Ω . We search for a solution $u \in H^1(\Omega)$ which satisfies the Poisson/Laplace equation at given proper boundary conditions: Dirchlet boundary conditions apply on $\Gamma_d \subset \Gamma$ and Neumann boundary conditions apply on $\Gamma_n := \Gamma \setminus \Gamma_d$.

The Poisson equation (named after its discoverer Simon-Denis Poisson) is of the form

$$-\Delta u = f \quad \text{in } \Omega \quad (2.1.1)$$

that satisfies Dirchlet boundary conditions

$$u = u_d \quad \text{on } \Gamma_d \quad (2.1.2)$$

and Neumann boundary conditions

$$\frac{du}{dn} = g \quad \text{on } \Gamma_n \quad (2.1.3)$$

where $f \in L^2(\Omega)$, $u_d \in H^1(\Omega)$ and $g \in L^2(\Gamma_n)$.

The Laplace equation (named after Pierre-Simon Laplace) is defined as

$$\Delta u = 0 \quad \text{in } \Omega \quad (2.1.4)$$

The same boundary conditions apply as for the Poisson equation.

2.2 The Weak Formulation

The weak formulation (often also called variational formulation) is the starting point in finite element analysis. The Poisson equation is recast in the weak form by multiplying it by an arbitrary weight function w

$$w \in H_D^1(\Omega) := \{w \in H^1(\Omega) | w = 0 \text{ on } \Gamma_D\} \quad (2.2.1)$$

with H^1 the standard Sobolev space which is also the Ansatz function and integrating over the domain of the problem Ω ,

$$-\int_{\Omega} \Delta u \cdot w dv = \int_{\Omega} f \cdot w dv. \quad (2.2.2)$$

By using the vector derivative identity

$$\nabla \cdot (w \nabla u) = w \Delta u + (\nabla u) \cdot (\nabla w) \quad (2.2.3)$$

and using the divergenz theorem

$$\int_{\Omega} \nabla \cdot (F) dv = \int_{\Gamma} F \cdot da \quad (2.2.4)$$

the weak formulation of the Poisson Problem is derived

$$\int_{\Omega} \nabla u \cdot \nabla w dv - \int_{\Gamma} w \cdot \frac{du}{dn} da = \int_{\Omega} f \cdot w dv. \quad (2.2.5)$$

2.3 The Galerkin Discretization

In order to solve the Poisson problem numerically, the weak formulation is discretised with a linear basis function η with a set of linear basis vectors (η_1, \dots, η_N) , where N is the dimension of the solution space S of U . Furthermore the weighted residual function w is redefined and the finite element solution U is developed in a serial

expansion in terms of the linear basis function η

$$\begin{aligned} w &= \eta_j \\ U &= \sum_k u_k \eta_k. \end{aligned} \quad (2.3.1)$$

Inserting Equations 2.3.1 into the weak formulation of the Poisson equation 2.2.5, we obtain

$$\int_{\Omega} (\nabla \sum_k u_k \eta_k) \cdot \nabla \eta_j dv - \int_{\Gamma} g \cdot \eta_j da = \int_{\Omega} f \cdot \eta_j dv \quad (2.3.2)$$

which can be rewritten to

$$\sum_k u_k \int_{\Omega} \nabla \eta_k \cdot \nabla \eta_j dv - \int_{\Gamma} g \cdot \eta_j da = \int_{\Omega} f \cdot \eta_j dv \quad (2.3.3)$$

and simplified to a system of linear equations

$$A \cdot U = b \quad (2.3.4)$$

where A is the Stiffness Matrix

$$A_{jk} = \int_{\Omega} \nabla \eta_k \cdot \nabla \eta_j dv \quad (2.3.5)$$

and b the Right Hand Side of the system of linear equations

$$b_j = \int_{\Omega} f \cdot \eta_j dv + \int_{\Gamma} g \cdot \eta_j da \quad (2.3.6)$$

The stiffness matrix A is sparse, symmetric and positive definite resulting in 1 solution of the system of linear equations 2.3.3 has in \mathbb{R}^3 , which gives the Galerkin solution

$$U = \sum_k u_k \eta_k. \quad (2.3.7)$$

2.4 Boundary Element Method

The basic steps in the boundary element method are quiet similar to the finite element method. First a integral equation has to be formed from the Poisson equation by using a weighted integral equation and then using the Green-Gauss theorem

$$\int_{\Omega} \nabla u \cdot \nabla w dv - \int_{\Gamma} w \cdot \frac{du}{dn} da = \int_{\Omega} f \cdot w dv. \quad (2.4.1)$$

Equation 2.4.1 is the starting equation of the finite element method. To derive the starting equation for the boundary element method the Green-Gauss theorem is applied again on the second integral, which gives

$$\int_{\Omega} \nabla u \cdot \nabla w dv - \int_{\Gamma} w \cdot \frac{du}{dn} da = \quad (2.4.2)$$

$$- \int_{\Omega} u \cdot \Delta w dv + \int_{\Gamma} u \cdot \frac{dw}{dn} da - \int_{\Gamma} w \cdot \frac{du}{dn} da = \int_{\Omega} f \cdot w dv. \quad (2.4.3)$$

In the Galerkin FEM the weight residual function was set to η , one of the basis functions used to approximate the solution u . For the boundary element method w is the fundamental solution of the Poisson equation in \mathbb{R}^N . For $N = 3$ the weighted residual function w is

$$w = \frac{1}{4\pi r} \quad (2.4.4)$$

where $r = \sqrt{(\alpha - x)^2 + (\beta - x)^2 + (\gamma - x)^2}$ and is singular at the point $(\alpha, \beta, \gamma) \in \Omega$. Taking from Equation 2.4.3 the domain integral and using the property of the Dirac delta function on it

$$\int_{\Omega} u \cdot \Delta w dv = \quad (2.4.5)$$

$$- \int_{\Omega} u \cdot \delta(\alpha - x, \beta - y, \gamma - z) dv = -u(\alpha, \beta, \gamma) \quad (\alpha, \beta, \gamma) \in \Omega \quad (2.4.6)$$

replaces the integral by a point value. Using this expression in 2.4.2 recasts it to

$$u(\alpha, \beta, \gamma) + \int_{\Gamma} u \cdot \frac{dw}{dn} da = \int_{\Gamma} w \cdot \frac{du}{dn} da + \int_{\Omega} f \cdot w dv. \quad (\alpha, \beta, \gamma) \in \Omega \quad (2.4.7)$$

For the Laplace equation $f = 0$ applies and the last term of the right hand side of equation 2.4.7 vanishes. Then the equation contains only boundary integrals and is referred to as a boundary integral equation. The values of u can relate either to points inside the solution domain or to points on the boundary of the solution domain. In the later case, one has to calculate the limit $(\alpha, \beta, \gamma) \rightarrow \Gamma$ and it is necessary to distinguish if the point is at a smooth boundary position (i.e. point with a unique tangent) or at a not smooth boundary position (i.e. a corner).

Taking these considerations into account, a generalized expression can be defined with P denoting the point (α, β, γ)

$$c(P)u(P) + \int_{\Gamma} u \cdot \frac{dw}{dn} da = \int_{\Gamma} w \cdot \frac{du}{dn} da. \quad (\alpha, \beta, \gamma) \in \Omega \quad (2.4.8)$$

where

$$c(P) = \begin{cases} 1 & \text{if } P \in \Omega \\ \frac{1}{2} & \text{if } P \in \Gamma \text{ and } \Gamma \text{ smooth at } P \\ \frac{\Theta}{2\pi} & \text{if } P \in \Gamma \text{ and } \Gamma \text{ not smooth at } P \end{cases} \quad (2.4.9)$$

with Θ being the inner solid angle.

Equation 2.4.8 involves only the surface contributions of u and $\frac{du}{dn}$ at the point P . Once these surface contributions are known, the value of u on any point P inside the region Ω can be calculated.

Thus the major advantage of the boundary element method compared to the finite element method is that the overall size of the problem is reduced by one dimension (from volumes to surfaces). But the major drawback of the boundary element method is that a fundamental solution must be found in the first place and there a many linear problems (e.g. nonhomogeneous equations) for which fundamental solutions are not known.

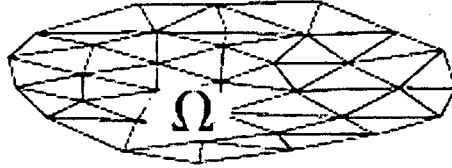


Figure 2.1: Domain of interest is divided into triangular elements (2D).

2.5 Mesh Generation

In the finite element method, the domain of interest is divided into a set of connected basic elements (e.g. triangles, tetrahedrons, etc), this process being called a regular triangulation, see Fig.2.1 To achieve a regular triangulation with finite elements several conditions have to be taken into account which were defined by Ciarlet [1]

- The vertices of the mesh coincide with the points where the basis function is one.
- The elements of the triangulation do not overlap.
- Each face on the surface of the body belongs either to Γ_D or Γ_N .

The creation of 3-dimensional geometries and the mesh are done with sophisticated commercial software such as GID [2]. Once a regular triangulation T was generated, a proper basis function for the solution space S of the numerical solution U in the domain Ω has to be chosen. The Hat function is a very common choice as a basis function for the space S , see Fig.2.2, which is defined for every node (x_j, y_j, z_j) of the finite element mesh

$$\eta_j(x_k, y_k, z_k) = \delta_{jk} \quad (j, k = 1, \dots, N). \quad (2.5.1)$$

As the Galerkin discretization uses isoparametric elements, the same polynomials (linear basis functions) for the approximation of the geometry and the solution are

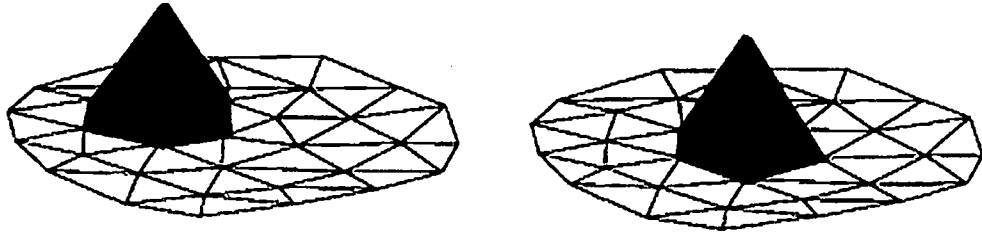


Figure 2.2: Hat-function.

used, and it is very easy to construct the stiffness matrix A and the right hand side b as the sum over all elements T and surface triangles E .

$$A_{jk} = \sum_{T \in \mathcal{T}} \int_T \nabla \eta_j \cdot \nabla \eta_k dv \quad (2.5.2)$$

and b the right hand side of the system of linear equations

$$b_j = \sum_{T \in \mathcal{T}} \int_T f \cdot \eta_j + \sum_{E \in \mathcal{E}} \int_E g \cdot \eta_j da. \quad (2.5.3)$$

The stiffness matrix is calculated on an element by element basis, and afterwards the contributions to the local matrix are assembled to a global stiffness matrix.

If the vertices of a tetrahedron element T are given by $(x_{j'}, y_{j'}, z_{j'})$ with j' ranging from 1 to 4 then the volume of the element $|T|$ will be defined as follows

$$|T| = \frac{1}{6} \det \begin{pmatrix} 1 & x_{j'} & y_{j'} & z_{j'} \\ 1 & x_{j'+1} & y_{j'+1} & z_{j'+1} \\ 1 & x_{j'+2} & y_{j'+2} & z_{j'+2} \\ 1 & x_{j'+3} & y_{j'+3} & z_{j'+3} \end{pmatrix} \quad (2.5.4)$$

where the local numbering j' of the element is chosen in such a way that the right hand side of equation 2.5.4 will be positive.

In order to evaluate the contribution of each finite element to the stiffness matrix,

so-called shape functions are introduced on each tetrahedron T :

$$\eta_{j'}^T(x_{k'}, y_{k'}, z_{k'}) = \delta_{j'k'} \quad (j', k' = 1, \dots, 4) \quad (2.5.5)$$

recast in matrix form

$$\eta_{j'} = \det \begin{pmatrix} 1 & x & y & z \\ 1 & x_{j'+1} & y_{j'+1} & z_{j'+1} \\ 1 & x_{j'+2} & y_{j'+2} & z_{j'+2} \\ 1 & x_{j'+3} & y_{j'+3} & z_{j'+3} \end{pmatrix} \setminus \det \begin{pmatrix} 1 & x_{j'} & y_{j'} & z_{j'} \\ 1 & x_{j'+1} & y_{j'+1} & z_{j'+1} \\ 1 & x_{j'+2} & y_{j'+2} & z_{j'+2} \\ 1 & x_{j'+3} & y_{j'+3} & z_{j'+3} \end{pmatrix} \quad (2.5.6)$$

and its derivative

$$\nabla \eta_{j'}(x, y, z) = \frac{1}{6|T|}$$

$$\begin{pmatrix} y_{j'+2}z_{j'+1} - y_{j'+3}z_{j'+1} - y_{j'+1}z_{j'+2} + y_{j'+3}z_{j'+2} + y_{j'+1}z_{j'+3} - y_{j'+2}z_{j'+3} \\ -x_{j'+2}z_{j'+1} + x_{j'+3}z_{j'+1} + x_{j'+1}z_{j'+2} - x_{j'+3}z_{j'+2} - x_{j'+1}z_{j'+3} + x_{j'+2}z_{j'+3} \\ x_{j'+2}y_{j'+1} - x_{j'+3}y_{j'+1} - x_{j'+1}y_{j'+2} + x_{j'+3}y_{j'+2} + x_{j'+1}y_{j'+3} - x_{j'+2}y_{j'+3} \end{pmatrix} \quad (2.5.7)$$

and with all indices understood as modulo 4, the contribution of element T to the stiffness matrix entries can be calculated

$$A_{j'k'}^T = \int_T \nabla \eta_{j'} \cdot (\nabla \eta_{k'}) dv. \quad (2.5.8)$$

Using a mapping from the finite element number and the local node index to the global node index

$$(T, j') \rightarrow j, \quad (2.5.9)$$

the entries of the element stiffness matrix $A_{j'k'}^T$ are summed up to the global stiffness matrix A_{jk} . For the right hand side of Equation 2.5.3 the first term is evaluated by transforming the coordinates into the center of gravity which allows the approximation

$$\int_T f \cdot \eta_j \approx \frac{|T|}{4} f(x_s, y_s, z_s) \quad (2.5.10)$$

and the second term can be evaluated in a similar way.

Dirchlet boundary conditions can be implemented by replacing their non-diagonal values in the matrix with zero, the diagonal values with unity and incorporating the known node entries in the right hand side.

Chapter 3

Principles of Magnetization Motion

In this chapter the equations which are needed to describe the magnetic motion of magnetic spins as well as the magnetization rate of change will be presented, laying emphasis on the intimate links between quantum mechanical concepts and the parameters employed in applied magnetism. The analysis of magnetization motion starts by considering an *ab initio* formulation to derive the gyromagnetic equation for a single spin. Through the introduction of spatial degrees of freedom a unified and self contained three dimensional variational approach for the general form of the equation of motion is derived. From the general form the well known Browns equations, including the general surface contributions and the underlying boundary conditions from volume interactions can be deduced. At last damping is introduced in a phenomenological way, leading to the well known Landau–Lifshitz–Gilbert equation of magnetization motion. The contribution of eddy currents on the magnetization dynamics will be discussed in the following chapters in detail, but for now shall be mentioned here only by introducing a modified damping parameter.

3.1 Quantum-Mechanical Concepts

A magnetic moment \mathbf{M} is associated with the electrons angular momentum \mathbf{L} and the same can be assumed for the electrons spin [3]. The relation between the electrons spin and its intrinsic magnetic moment is given by

$$\mathbf{M} = \gamma \mathbf{S} \quad (3.1.1)$$

where γ is the gyromagnetic ratio and is expressed as

$$\gamma = \frac{g\mu_B}{\hbar} < 0 \quad (3.1.2)$$

with g being the gyromagnetic splitting factor or Landé factor and \hbar the Planks constant. In context with equation 3.1.2 the Bohr magneton μ_B

$$\mu = \frac{q_e \hbar}{2m_e} \quad (3.1.3)$$

with q_e and m_e the charge and the mass of the electron, respectively has to be negative.

To determine the magnetic moment \mathbf{M} correctly, the electrons total angular momentum \mathbf{J} consisting of the angular momentum \mathbf{L} and the spin \mathbf{S} , $\mathbf{J} = \mathbf{L} + \mathbf{S}$, has to be taken into account. Once Equation 3.1.1 is modified accordingly, based on the quantum mechanical theory of angular momentum, a general expression for the Landé g can be obtained

$$g = \frac{3}{2} + \frac{S(S+1) - L(L+1)}{2J(J+1)}. \quad (3.1.4)$$

Depending on material properties the gyromagnetic splitting factor can be approximated to be either equal to 1, which is the case for spinless particles ($S = 0$, $J = L$), or equal to 2, which is the fact when all orbital contributions to the angular momentum are disregarded ($S = J$, $L = 0$). The latter case is most common for ferromagnetic metals, as the orbital contributions are found to be rather small, which was shown

by C. T. Chen et al. [4] who investigated the quantitative values of orbital to spin magnetic moment ratios.

The time evolution of the mean value of quantum mechanical operators associated with measurable physical quantities provides the link between quantum and classical mechanics. Such an operator is called an observable.

The mean value $\langle A \rangle$ of an observable A evolves in time according to the Schrödinger equation

$$\frac{d}{dt}\langle A \rangle = \frac{1}{i\hbar}\langle [A, H] \rangle + \left\langle \frac{\partial A}{\partial t} \right\rangle \quad (3.1.5)$$

where H is the Hamiltonian operator.

Having defined a general expression for the time evolution of an observable, it is possible to determine the time evolution of the magnetic moment \mathbf{M} in an arbitrary external magnetic field. Since \mathbf{M} does not explicitly depend on time the second term in equation 3.1.5 vanishes and the mean value is expressed as

$$\frac{d}{dt}\langle M_i \rangle = \frac{1}{i\hbar}\langle [M_i, H] \rangle, \quad i = x, y, z \quad (3.1.6)$$

with the Hamiltonian $H = -\mathbf{M} \cdot \mathbf{B}$.

To derive the precession movement of the spin, the x component of the commutator in equation 3.1.6 has to be expanded and bearing in mind that \mathbf{B} is a classical quantity, yields

$$\begin{aligned} [M_x, H] &= -\gamma^2[S_x, S_x B_x + S_y B_y + S_z B_z] \\ &= -\gamma^2 B_y [S_x, S_y] - \gamma^2 B_z [S_x, S_z]. \end{aligned} \quad (3.1.7)$$

$$\begin{aligned} [M_y, H] &= -\gamma^2[S_y, S_x B_x + S_y B_y + S_z B_z] \\ &= -\gamma^2 B_x [S_y, S_x] - \gamma^2 B_z [S_y, S_z]. \end{aligned} \quad (3.1.8)$$

$$\begin{aligned} [M_z, H] &= -\gamma^2[S_z, S_x B_x + S_y B_y + S_z B_z] \\ &= -\gamma^2 B_x [S_z, S_x] - \gamma^2 B_y [S_z, S_y]. \end{aligned} \quad (3.1.9)$$

The Spin is an angular momentum operator and obeys the usual commutation rules

$$\begin{aligned} [S_x, S_y] &= i\hbar S_z \\ [S_y, S_z] &= i\hbar S_x \\ [S_z, S_x] &= i\hbar S_y \end{aligned} \quad (3.1.10)$$

which are substituted into Equations 3.1.7-3.1.9 and one obtains

$$\begin{aligned} [M_x, H] &= i\hbar\gamma^2(B_z S_y - B_y S_z) \\ [M_y, H] &= i\hbar\gamma^2(B_x S_z - B_z S_x) \\ [M_z, H] &= i\hbar\gamma^2(B_x S_y - B_y S_x). \end{aligned} \quad (3.1.11)$$

The cyclic permutation as shown above allows to recast Equation 3.1.6 to

$$\frac{d}{dt}\langle \mathbf{M} \rangle = \gamma(\langle \mathbf{M} \rangle \times \mathbf{B}). \quad (3.1.12)$$

Equation 3.1.12 gives the time evolution of the mean value of the magnetic moment \mathbf{M} in an arbitrary external field. The classical equivalent can be expressed in terms of the magnetization \mathbf{M} , by being defined as the magnetic moment, and applying for $\mathbf{B} = \mu_0 \mathbf{H}$

$$\frac{d\mathbf{M}}{dt} = \mu_0 \gamma (\mathbf{M} \times \mathbf{H}). \quad (3.1.13)$$

Furthermore the gyromagnetic constant γ and the permeability of free space μ_0 can be lumped into a new gyromagnetic constant γ_0

$$\gamma_0 = -\mu_0 \gamma > 0 \quad (3.1.14)$$

which applied to the equation 3.1.13 results in the well known form for the precessional motion of the magnetization

$$\frac{d\mathbf{M}}{dt} = -\gamma_0 (\mathbf{M} \times \mathbf{H}). \quad (3.1.15)$$

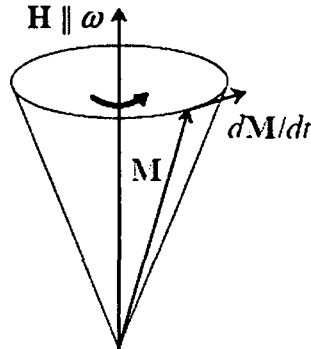


Figure 3.1: Precessional motion of magnetization.

The applied field can be either time independent or time dependent. The first case results in a constant precession of the magnetization vector and a constant angle between the magnetic field and the magnetization, meaning that the energy $-\mu(\mathbf{M} \cdot \mathbf{H})$ remains unchanged, which can be easily shown by multiplying Equation 3.1.15 successively with \mathbf{H} and \mathbf{M}

$$\frac{d}{dt}(\mathbf{M} \cdot \mathbf{H}) = 0 \quad \text{and} \quad \frac{d}{dt}(M^2) = 0. \quad (3.1.16)$$

For the dependant case the applied field is substituted with the angular velocity vector $\boldsymbol{\omega} = \gamma_0 \mathbf{H}$

$$\frac{d\mathbf{M}}{dt} = -(\mathbf{M} \times \boldsymbol{\omega}). \quad (3.1.17)$$

and describes the precessional motion of the magnetization vector around $\boldsymbol{\omega}$. Figure 3.1 visualizes Equation 3.1.17 and shows that $d\mathbf{M}/dt$ lies continuously in a plane perpendicular to the angular velocity vector describing an instantaneous precessional motion of magnetization.

3.2 Lagrangian Formulation of the Equation of Motion

In the last section the precessional motion of the magnetization vector was derived. So far, no transfer of the kinetic and potential energy associated with macroscopic motion to kinetic energy of microscopic thermal motion has been taken into account. For a magnetization field this transfer can be either through microscopic thermal motion of spin waves or through a coupled or associated field, like strain fields or the eddy current. The details of the transfer mechanism are too complex to be introduced into the field equations explicitly. To include these transfer mechanisms into the field equations a phenomenological damping term is introduced. The different contributions to damping contained in this damping term have to be determined experimentally.

In principle a damping of a physical system generates a force in opposition to the macroscopic driving force. A steady state is maintained when, the energy gain from the driving force is balanced by the energy loss from the damping force. If the forces are not equal, energy is either gained (if the driving force is larger) or lost (if the damping force is larger), which results in an acceleration or deceleration of the macroscopic motion, respectively.

In the simplest case where many different damping forces but no resonance phenomena occur, the damping force is proportional to the rate of change of the magnetization field of the system.

3.2.1 Lagrangian formulation

A common way to introduce such a damping term is to use the Lagrangian formulation of the equation of motion and adding a velocity dependant term which is derived from

a quadratic function of the time derivatives of components of the magnetization field, the Rayleighs dissipation function[5].

Given the magnetization field $\mathbf{M} = \mathbf{M}(\mathbf{r}, t)$, the equation of motion of an undamped magnetization field in Lagrangian form is given by

$$\frac{d}{dt} \frac{\delta L[\mathbf{M}, \dot{\mathbf{M}}]}{\delta \dot{\mathbf{M}}} - \frac{\delta L[\mathbf{M}, \dot{\mathbf{M}}]}{\delta \mathbf{M}} = 0. \quad (3.2.1)$$

The Lagrangian of the magnetization field is defined as follows

$$L[\mathbf{M}, \dot{\mathbf{M}}] = T[\mathbf{M}, \dot{\mathbf{M}}] - U[\mathbf{M}] \quad (3.2.2)$$

with T being the kinetic and U the potential energy.

By adding a dissipative force term

$$\frac{\delta R[\dot{\mathbf{M}}]}{\delta \dot{\mathbf{M}}} \quad (3.2.3)$$

to Equation 3.2.1 an equation for a damped magnetization field is derived

$$\frac{d}{dt} \frac{\delta L[\mathbf{M}, \dot{\mathbf{M}}]}{\delta \dot{\mathbf{M}}} - \frac{\delta L[\mathbf{M}, \dot{\mathbf{M}}]}{\delta \mathbf{M}} + \frac{\delta R[\dot{\mathbf{M}}]}{\delta \dot{\mathbf{M}}} = 0. \quad (3.2.4)$$

R is a Rayleigh dissipation functional and is defined

$$R[\dot{\mathbf{M}}] = \frac{\eta}{2} \int \dot{\mathbf{M}} \cdot \dot{\mathbf{M}} d^3r \quad (3.2.5)$$

with η being the average damping parameter for the sample, which is an approximation of the damping mechanisms. The functional R could be recast to take nonuniform damping into account but it would not be possible to calculate and measure all the variety of mechanisms that contribute to local damping.

Substituting the Lagrangian expression into Equation 3.2.4, to separate the kinetic and potential energy contributions and using the following identities

$$\frac{\delta U[\mathbf{M}]}{\delta \mathbf{M}} = 0 \quad (3.2.6)$$

$$\frac{\delta R[\dot{\mathbf{M}}]}{\delta \dot{\mathbf{M}}} = \eta \dot{\mathbf{M}} \quad (3.2.7)$$

one obtains an expression for a dampened magnetization motion

$$\frac{d}{dt} \frac{\delta T[\mathbf{M}, \dot{\mathbf{M}}]}{\delta \dot{\mathbf{M}}} - \frac{\delta T[\mathbf{M}, \dot{\mathbf{M}}]}{\delta \mathbf{M}} - \frac{\delta U[\mathbf{M}]}{\delta \mathbf{M}} + \eta \dot{\mathbf{M}} = 0. \quad (3.2.8)$$

3.2.2 Landau–Lifshitz–Gilbert Equation

Equation 3.2.8 imposes the problem that the kinetic energy T of the classical Lagrangian depends on dynamical variables that are not defined for quantum spin operators which makes it impossible to derive an expression for the kinetic energy of a rotating body in classical mechanics that corresponds to the spin of an elementary particle in quantum mechanics.

But an approximation can be gained if we set the damping parameter η equal to zero. In this case the remaining terms of Equation 3.2.8 can be compared with Equation 3.1.13. Further the added damping term in 3.2.8 can be looked at as a damping field that reduces the effective field and changes the torque exerting on the magnetization field. Then one can argue that by adding the same damping term to the effective field in 3.1.13 a comparable equation of motion for a damped magnetization field is obtained.

This equation can be written in the following form

$$\frac{\partial \mathbf{M}}{\partial t} = \mu_0 \gamma \mathbf{M} \times \left[\mathbf{H} - \eta \frac{\partial \mathbf{M}}{\partial t} \right]. \quad (3.2.9)$$

The form of Equation 3.2.9 is due to Gilbert [6]. It can be shown to be equivalent to the older form due to Landau and Lifshitz [16] by multiplying both sides of Equation 3.2.9 with $\mathbf{M} \times$ yielding

$$\mathbf{M} \times \frac{\partial \mathbf{M}}{\partial t} = \mathbf{M} \times \left(\mu_0 \gamma \mathbf{M} \times \left[\mathbf{H} - \eta \frac{\partial \mathbf{M}}{\partial t} \right] \right). \quad (3.2.10)$$

The second term on the right hand side can be recast by making use of the following vector identity

$$M_s^2 \frac{\partial \mathbf{M}}{\partial t} = \mathbf{M} \left(\mathbf{M} \cdot \frac{\partial \mathbf{M}}{\partial t} \right) - \mathbf{M} \times \left(\mathbf{M} \times \frac{\partial \mathbf{M}}{\partial t} \right) \quad (3.2.11)$$

with $|\mathbf{M}| = M_s$. Inserting this vector identity in Equation 3.2.10 and applying the new expression to 3.2.9 yields

$$\frac{\partial \mathbf{M}}{\partial t} = \mu_0 \gamma \mathbf{M} \times \mathbf{H} - (\mu_0 \gamma)^2 \eta \mathbf{M} \times (\mathbf{M} \times \mathbf{H}) - (\mu_0 \gamma)^2 \eta^2 M_s^2 \frac{\partial \mathbf{M}}{\partial t}. \quad (3.2.12)$$

Rearranging the terms in Equation 3.2.12 and using the gyromagnetic constant γ_0 from 3.1.14 leads to the old form of the Landau–Lifshitz equation

$$\frac{\partial \mathbf{M}}{\partial t} = -\dot{\gamma}_0 \mathbf{M} \times \mathbf{H} - \lambda \mathbf{M} \times (\mathbf{M} \times \mathbf{H}) \quad (3.2.13)$$

with

$$\dot{\gamma}_0 = \frac{\gamma_0}{1 + \gamma_0^2 \eta^2 M_s^2} \quad \text{and} \quad \lambda = \frac{\gamma_0^2 \eta}{1 + \gamma_0^2 \eta^2 M_s^2}. \quad (3.2.14)$$

Taking the above presented equation but using the Gilbert constant α and the gyromagnetic constant γ_0

$$\alpha = \gamma_0 \eta M_s \quad (3.2.15)$$

the usually designated Landau–Lifshitz–Gilbert equation of magnetization motion is obtained

$$(1 + \alpha^2) \frac{\partial \mathbf{M}}{\partial t} = -\gamma_0 (\mathbf{M} \times \mathbf{H}) - \gamma_0 \frac{\alpha}{M_s} \mathbf{M} \times (\mathbf{M} \times \mathbf{H}). \quad (3.2.16)$$

Chapter 4

Micromagnetics

The history of micromagnetics starts with a paper of Landau and Lifshitz on the structure of a wall between two antiparallel domains published in the year 1935, and with several papers written by Brown in 1940. A detailed treatment of micromagnetism is given by Brown in his 1963 book [8]. In the following years micromagnetics was limited to the use of standard energy minimization approaches to determine domain structures and the classical nucleation theory was used to determine magnetization reversal mechanisms in regimes with an ideal geometry. Starting in the mid-1980s an increased interest in micromagnetism due to the availability of large-scale computing power was investigated which enabled the study of more realistic problems more comparable with experimental data. One of the first achievements was the fact that energy minimization addresses in principle only specific nucleation fields for the selected system and not the state of the regime after magnetization reversal. Therefore, a lot of research was done in the development of dynamic approaches using simulations based on the Landau and Lifshitz equation of motion, which is the most common technique in use today. Another important part of micromagnetic calculations is the development of techniques to calculate magnetostatic fields, low frequency field approximations.

Micromagnetism is a continuum theory to describe magnetization processes on a significant length scale which is large enough to replace atomistic magnetic moments by a continuous function of position and small enough to reveal the transitions between magnetic domains [9]. Due to the rapid increase in computational power numerical micromagnetics has become an essential tool to characterize magnetic materials as used in high density magnetic recording and magneto-electronics [10]. The precise understanding of the magnetization reversal process is essential in the development of ultrahigh density storage media [11] and magneto-electronic devices [12]. The numerical integration of the equations of motion, which describe the dynamic response of a magnetic system under the influence of an external field, provides a detailed understanding of the microscopic processes that determine the macroscopic magnetic properties like switching time and switching field. In addition to external parameters like the applied magnetic field and the temperature, the magnetization reversal process significantly depends on the interplay between the physical/chemical microstructure of a magnet and the local arrangement of the magnetic moments.

A very important tool in micromagnetics is the finite element method which is a highly flexible application that helps to describe magnetization processes in more detail, since it is possible to incorporate the physical grain structure and to adjust the finite element mesh according to the local magnetization. An efficient error indicator can be defined by making use of a conservation law inherent to the physics of the problem. In order to treat the magnetostatic interactions of distinct magnetic parts, the finite element method can be combined with a boundary element method. The discretization of space of the partial differential equations which govern the magnetization dynamics leads to a stiff system of ordinary differential equations. To reduce the calculation time for time integration of the combined set of differential equations, preconditioned backward differentiation methods are used rather than Adams or Runge-Kutta methods.

4.1 Basic Principles of Micromagnetics

The basic concept of micromagnetism is to replace the atomic magnetic moment by a continuous function of position. As mentioned before in continuum theory the local direction of the magnetization moment can be described by a polarization vector

$$\mathbf{J} = \mu_0 \mathbf{M} = \mu_0 \frac{\mathbf{m}}{V} \quad (4.1.1)$$

where the magnetic polarization \mathbf{J} is proportional to the magnetization \mathbf{m} per unit volume V , μ_0 being the magnetic permeability of vacuum.

In the following sections the magnetization \mathbf{M} will be used rather than \mathbf{J} and the magnetization is assumed to be a continuous vector-field $\mathbf{M}(\mathbf{r})$.

$$\mathbf{M}(\mathbf{r}) = M_s \frac{\mathbf{m}(\mathbf{r})}{|\mathbf{m}|} \quad (4.1.2)$$

with \mathbf{r} the position vector and M_s the saturation magnetization of the material.

The second principle of micromagnetism treats the magnitude of the magnetization only as a function of the temperature. The modulus of \mathbf{M} is

$$|\mathbf{M}| = M_s(T) \quad (4.1.3)$$

defined to be a function of temperature and independent of the local magnetic field, which allows to describe the magnetic state of a system uniquely by the direction cosines $\mathbf{b}(\mathbf{r})$ of the magnetization

$$\mathbf{M} = \mathbf{b}(\mathbf{r}) M_s. \quad (4.1.4)$$

In a meta-stable equilibrium state the direction cosines minimize the total Gibbs free energy of the system.

4.2 Total magnetic Gibbs free Energy

The total magnetic Gibbs free energy consists of several energy contributions which are derived from classical electrodynamics, condensed matter physics, and quantum

mechanics. The aim is to derive a continuous expressions for the energy that describes the interactions of the spins with the external field, the crystal lattice, and the interactions of the spins with one another. The latter consists of long-range magnetostatic interactions and short-range quantum-mechanical exchange interactions. The equilibrium distribution of the magnetization is determined by the minimization of the competitive effects of the micromagnetic energy contributions: anisotropy energy, exchange energy, magnetostatic fields and Zeeman energy.

4.2.1 Anisotropy Energy

The anisotropy term refers to the fact that the properties of a magnetic material are dependent on the directions in which they are measured. The anisotropy itself has a number of possible origins such as: **crystal magneto-crystalline anisotropy**, **shape anisotropy** and **stress anisotropy**.

magneto-crystalline anisotropy

The magneto-crystalline anisotropy is an intrinsic contribution of the material having its origin in the atomic level. For materials with a large anisotropy a strong coupling between the orbital angular momentum and the spin can be observed, which results in a non-spherical shape of the atomic orbital.

Due to this shape the orbits prefer to lie in certain crystallographic directions. The spin-orbit coupling then assures a preferred direction for the magnetization called the easy direction. To rotate the magnetization away from the easy direction consumes energy, anisotropy energy. As might be expected the anisotropy energy depends on the lattice structure.

The energy term for uniaxial anisotropy, found in hexagonal crystals like Cobalt

(Co) is given by

$$E = KV \sin^2 \theta + \text{higher terms.} \quad (4.2.1)$$

Here θ being the angle between the easy direction and the magnetization, K being the anisotropy constant, V the volume of the sample and the higher terms are normally neglected as their contribution is small. This system with one easy direction has two energy minima separated by an energy maximum, resulting in an energy barrier that leads to hysteresis.

For cubic anisotropy, found in Iron and Nickel the energy term will be given by the following expression

$$E = K_0V + K_1V(b_1^2b_2^2 + b_2^2b_3^2 + b_1^2b_3^2) \quad (4.2.2)$$

where b_i are the direction cosine, the cosine of the angle between the magnetization direction and the easy axis, respectively.

shape anisotropy

The shape anisotropy can be described in analogy with dielectric materials by referring to the magnetization producing fictitious free poles at the surface, which leads to a demagnetization field \mathbf{H}_d that opposes \mathbf{M} . Figure 4.1 shows a sample with an anisotropic shape with a magnetic field applied in two perpendicular directions.

The energy increases with increasing demagnetization field H_d . For an ellipsoid of revolution it can be shown that the energy is

$$E = -K_{\text{eff}} \sin \theta \quad (4.2.3)$$

and has the same form as the uniaxial anisotropy with θ being the angle between the long axis of the sample and the magnetization direction and the K_{eff} is an expression

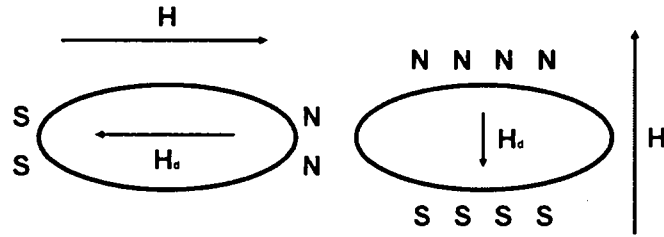


Figure 4.1: Sample with an anisotropic shape with a magnetic field applied in two perpendicular directions: (right) parallel to the short axis; here the free poles are separated by a relatively short distance, leading to a large \mathbf{H}_d , (left) parallel to the long axis; poles separated by a smaller distance, which leads to a small value of \mathbf{H}_d .

based on the demagnetization factors of the long N_a and short N_b axis of the sample and the magnetization M_s

$$K_{\text{eff}} = \frac{1}{2}(N_b - N_a)\mu_0 M_s^2. \quad (4.2.4)$$

The demagnetization factors N_a and N_b are geometry dependent so that K_{eff} for sphere is

$$K_{\text{eff}} = 0 \quad (4.2.5)$$

and for a needle like geometry is

$$K_{\text{eff}} = -\mu_0 \frac{M_s^2}{2}. \quad (4.2.6)$$

stress anisotropy

In addition to magnetocrystalline anisotropy, there is another effect related to spin-orbit coupling called magnetostriction, which is related to the phenomenon of stress anisotropy. Magnetostriction arises from the strain dependence of the anisotropy constants. Upon magnetization, a previously demagnetized crystal experiences a strain

that can be measured as a function of applied field along the principal crystallographic axes. A magnetic material will therefore change its dimension when magnetized.

The inverse affect, the change of magnetization with stress as well occurs. A uniaxial stress can produce a unique easy axis of magnetization if the stress is sufficient to overcome all other anisotropies. The magnitude of the stress anisotropy is described by two more empirical constants known as the magnetostriction constants and the level of stress.

4.2.2 Exchange Energy

The exchange energy forms an important part in the covalent bond of solids and in ferromagnetic coupling. The exchange energy between two spins is given by

$$E_{\text{exch}} = -2IS_1 \cdot S_2 \quad (4.2.7)$$

where I is the exchange Integral and S_1 and S_2 are atomic spins. This direct exchange coupling is an idealization and applicable only to a few materials. Many other models exist such as itinerant electron ferromagnetism and indirect exchange interaction or Ruderman-Kittel-Kasuya-Yoshida (RKKY) interaction. However, Equation 4.2.7 is the form usually taken for the exchange interaction where the value of I depends on the detailed atomic properties of the material.

To actually calculate the exchange energy, one can take advantage of the fact that it is essentially short ranged and can be expressed by a summation of the nearest neighbors. Further assuming a slowly spatially varying magnetization the exchange energy can be written

$$E_{\text{exch}} = IS^2 \sum_i \sum_{j(nn)} \phi_{ij}^2 \quad (4.2.8)$$

with the summation carried out only over the nearest neighbors and where ϕ_{ij} represents the angle between the two neighboring spins i and j . Further it should be

mentioned that equation 4.2.8 gives the energy in reference to the energy state where all spins are aligned in the same direction. This approach is legal as long as it is done consistently.

Making the approximation for small angles that

$$\phi_{ij} \approx |\mathbf{b}_i - \mathbf{b}_j| \quad (4.2.9)$$

than the first order Taylor expansion gives

$$|\mathbf{b}_i - \mathbf{b}_j| = |(\mathbf{s}_i \cdot \nabla)\mathbf{b}_j| \quad (4.2.10)$$

where \mathbf{s}_i is a position vector joining lattice point i and j . Substituting 4.2.10 into 4.2.8 gives

$$E_{\text{exch}} = IS^2 \sum_i \sum_{j(nm)} |(\mathbf{s}_i \cdot \nabla)\mathbf{b}_j| \quad (4.2.11)$$

where the first sum is over all lattice points i and the second sum is over all nearest neighbors of i . The first summation can be transformed into a integral over the whole sample. The result is that for a cubic crystal

$$E_{\text{exch}} = \int_V \frac{IS^2}{a} \frac{1}{M_s^2} (\nabla \mathbf{M})^2 dV \quad (4.2.12)$$

with a being the lattice constant and $(\nabla \mathbf{M})^2$ is defined as

$$(\nabla \mathbf{M})^2 = (\nabla M_x)^2 + (\nabla M_y)^2 + (\nabla M_z)^2. \quad (4.2.13)$$

Equation 4.2.12 is an integral that relates fundamental atomic properties to the spatial derivation of the magnetization in the continuum approximation. The atomic properties are taken into account through the exchange I which is in micromagnetics terms a phenomenological constant that can be determined experimentally. By defining a constant A that includes all atomic properties, here for a cubic lattice

$$A = \frac{IS^2}{a} \quad (4.2.14)$$

the final expression for the exchange energy is derived

$$E_{\text{exch}} = \frac{1}{M_s^2} \int_V A(\nabla \mathbf{M})^2 dV \quad (4.2.15)$$

with A being called the exchange constant.

4.2.3 Magnetostatic Field

There are two kind of magnetostatic fields, one that arises from external sources which can be implemented easily and a second that arises from the magnetization distribution itself, which will be described in detail here. To calculate the magnetostatic or demagnetizing field \mathbf{H}_d one starts from Maxwell equations

$$\nabla \times \mathbf{H}_d = 0 \quad (4.2.16)$$

$$\nabla(\mathbf{H}_d + \mathbf{M}) = 0. \quad (4.2.17)$$

Since the curl of the demagnetizing field is zero it is possible to derive it from a scalar potential

$$\mathbf{H}_d = -\nabla\phi \quad (4.2.18)$$

and by substituting 4.2.18 into the governing Maxwell equations from above, one yields a diffusion equation for the scalar potential

$$\nabla^2\phi = \nabla \cdot \mathbf{M}. \quad (4.2.19)$$

Equation 4.2.19 is similar to the poisson equation in electrostatics which allows to define a volume magnetic charge density ρ

$$\rho = -\nabla \cdot \mathbf{M}. \quad (4.2.20)$$

Thus the magnetostatic field can be derived by solving 4.2.19 for the scalar potential that is subject to boundary conditions which determine the continuity of the normal

component of $\frac{1}{\mu_0}\mathbf{B} = \mathbf{H}_d + \mathbf{M}$ and of the tangential component of \mathbf{H}_d

$$\mathbf{n} \cdot (\mathbf{B}_{\text{out}} - \mathbf{B}_{\text{in}}) = 0 \quad (4.2.21)$$

$$\mathbf{n} \times (\mathbf{H}_{d;\text{out}} - \mathbf{H}_{d;\text{in}}) = 0 \quad (4.2.22)$$

where \mathbf{n} is a unit vector pointing outward from the surface.

In terms of the scalar potential the equivalent boundary conditions are

$$\phi_{\text{out}} = \phi_{\text{in}} \quad (4.2.23)$$

$$\left. \frac{\partial \phi}{\partial n} \right|_{\text{out}} - \left. \frac{\partial \phi}{\partial n} \right|_{\text{in}} = -\mathbf{M} \cdot \mathbf{n} \quad (4.2.24)$$

Although having its origins at the atomic level, the response of a magnetized body due to the magnetization distribution is governed by its surface, as shown above.

Having derived the governing equations and boundary conditions for the potential and demagnetizing field, they can be written as follows

$$\phi(\mathbf{r}) = -\frac{1}{4\pi\mu_0} \int_V \frac{\nabla \cdot \mathbf{M}(\mathbf{r}')}{|\mathbf{r} - \mathbf{r}'|} dV' + \frac{1}{4\pi\mu_0} \int_S \frac{\mathbf{M}(\mathbf{r}') \cdot \mathbf{n}}{|\mathbf{r} - \mathbf{r}'|} dS' \quad (4.2.25)$$

$$\mathbf{H}_d = -\frac{1}{4\pi\mu_0} \int_V \frac{(\mathbf{r} - \mathbf{r}') \nabla \cdot \mathbf{M}(\mathbf{r}')}{|\mathbf{r} - \mathbf{r}'|^3} dV' + \frac{1}{4\pi\mu_0} \int_S \frac{(\mathbf{r} - \mathbf{r}') \mathbf{M}(\mathbf{r}') \cdot \mathbf{n}}{|\mathbf{r} - \mathbf{r}'|^3} dS' \quad (4.2.26)$$

The integrals above can be interpreted as fields arising from volume and surface charges densities $\rho = -\nabla \cdot \mathbf{M}$ and $\sigma = \mathbf{M} \cdot \mathbf{n}$ respectively.

To finally calculate the total energy of the system it is necessary to integrate over the whole volume as follows

$$E_{\text{mag}} = \frac{1}{2} \int_V \mathbf{H}_d \cdot \mathbf{M} dV \quad (4.2.27)$$

which involves a six fold integration, meaning that although it is an elegant solution, it may not be the best form for numerical computation.

4.3 Browns Equations

The formulation of classical micromagnetics is achieved by minimization of the total energy. The aim is to achieve a minimum energy state for each single contributing

term, so that an overall energy minima is achieved. In some cases this can lead to competitive mechanisms, like with the ferromagnetic exchange energy and the magnetostatic energy, explained below.

The minimization of the ferromagnetic exchange energy aligns the magnetic moments parallel to each other, whereas the minimization of the magnetostatic energy favors the existence of magnetic domains. The magnetocrystalline anisotropy energy describes the interaction of the magnetization with the crystal lattice. Its minimization orients the magnetization preferably along certain crystallographic directions. The minimization of the Zeeman energy of the magnetization in an external field rotates the magnetization parallel to the applied field.

The to be to minimized total energy can be expressed as follows

$$E_{\text{tot}} = \int_V \left[\frac{A}{M_s^2} (\nabla \mathbf{M})^2 + E_{\text{anis}} - \mu_0 \mathbf{M} \cdot \left(\mathbf{H}_a + \frac{\mathbf{H}_d}{2} \right) \right] dV \quad (4.3.1)$$

where \mathbf{H}_a is the external applied field and E_{anis} , the anisotropy energy density.

The minimization approach uses standard variational principles. Setting the the first variation of the total energy with respect to the magnetization to zero results in two equations, a surface equation and a volume equation.

The surface equation from variational principle is

$$2A \left[\mathbf{b} \times \frac{\partial \mathbf{b}}{\partial n} \right] = 0 \quad \Rightarrow \quad \frac{\partial \mathbf{b}}{\partial n} = 0 \quad (4.3.2)$$

since $\mathbf{b} \cdot \frac{\partial \mathbf{b}}{\partial n} = 0$ by virtue of $\mathbf{b} \cdot \mathbf{b} = 1$. The volume equation is

$$\mathbf{b} \times \left[\frac{2A}{M_s} \nabla^2 \mathbf{b} + \mathbf{H}_d + \mathbf{H}_a + \mathbf{H}_{\text{anis}} \right] = 0 \quad (4.3.3)$$

where \mathbf{H}_{anis} , the anisotropy field, is defined as

$$\mathbf{H}_{\text{anis}} = -\frac{1}{M_s} \frac{\partial E_{\text{anis}}}{\partial \mathbf{b}}. \quad (4.3.4)$$

By recasting equation 4.3.3 one derives the following expression

$$\mathbf{b} \times \mathbf{H}_{\text{eff}} = 0 \quad (4.3.5)$$

with \mathbf{H}_{eff} being the effective field of the form

$$\mathbf{H}_{\text{eff}} = \frac{2A}{M_s} \nabla^2 \mathbf{b} + \mathbf{H}_d + \mathbf{H}_a + \mathbf{H}_{\text{anis}}. \quad (4.3.6)$$

Recapitulating the derivation shown above yields that the effective field H_{eff}

$$\mathbf{H}_{\text{eff}} = -\frac{\delta E_{\text{tot}}}{\delta \mathbf{M}} \quad (4.3.7)$$

is the negative variational derivative of the total magnetic Gibbs free energy.

The volume equation 4.3.3 states that the equilibrium solution is found by aligning the magnetization parallel to the local fields. The equation 4.3.2 to 4.3.6 are referred to as Brown's equations and form the basis of classical micromagnetic approach to the solution of stationary problems.

Chapter 5

Micromagnetics and LLG Equation

The aim of micromagnetic calculations is the better understanding of magnetic materials and their interaction with external fields. Breaking down the materials into atomic magnetic moments, the influence of external fields can be best described by the motion of the magnetic moments in these fields, by taking the properties of the materials into account.

In the last two chapters the basic tools, the Landau–Lifshitz–Gilbert equation of motion

$$\frac{\partial \mathbf{M}}{\partial t} = -\frac{\gamma_0}{(1 + \alpha^2)}(\mathbf{M} \times \mathbf{H}) - \gamma_0 \frac{\alpha}{M_s(1 + \alpha^2)}\mathbf{M} \times (\mathbf{M} \times \mathbf{H}) \quad (5.0.1)$$

and the total magnetic Gibbs free energy

$$E_{\text{tot}} = \int_V \left[\frac{A}{M_s^2}(\nabla \mathbf{M})^2 + E_{\text{anis}} - \mu_0 \mathbf{M} \cdot \left(\mathbf{H}_a + \frac{\mathbf{H}_d}{2} \right) \right] dV \quad (5.0.2)$$

whose negative variational derivative gives the effective field \mathbf{H}_{eff}

$$\mathbf{H}_{\text{eff}} = \frac{2A}{M_s} \nabla^2 \mathbf{b} + \mathbf{H}_{\text{anis}} + \mathbf{H}_d + \mathbf{H}_a \quad (5.0.3)$$

were derived. The first term is the exchange contribution \mathbf{H}_{exch} and the second is the anisotropy field \mathbf{H}_{anis} were defined in the previous chapter. The third and fourth term, the applied and the demagnetizing or magnetostatic field are calculated from

Maxwell equations [14]. The magnetostatic field \mathbf{H}_d is an irrotational field and is calculated by applying the magnetostatic potential ϕ into the conditional Maxwell equation

$$\nabla \cdot \mathbf{H}_d = -\nabla \cdot \mathbf{M} \quad (5.0.4)$$

$$\nabla \times \mathbf{H}_d = 0 \quad (5.0.5)$$

$$\nabla \cdot (\nabla \phi) = \nabla \cdot \mathbf{M}. \quad (5.0.6)$$

The equations above are solved using a method described by Fredkin and Koehler [13].

The applied field \mathbf{H}_a is a solenoidal field that is produced by external currents \mathbf{j}_a . The governing conditional equations are

$$\nabla \cdot \mathbf{H}_a = 0 \quad (5.0.7)$$

$$\nabla \times \mathbf{H}_a = \mathbf{j}_a. \quad (5.0.8)$$

By substituting 5.0.3 into 5.0.1 one obtains

$$\begin{aligned} \frac{\partial \mathbf{M}}{\partial t} = & -\frac{\gamma_0}{(1 + \alpha^2)} (\mathbf{M} \times (\frac{2A}{M_s} \nabla^2 \mathbf{b} + \mathbf{H}_d + \mathbf{H}_a + \mathbf{H}_{\text{anis}})) \\ & -\gamma_0 \frac{\alpha}{M_s(1 + \alpha^2)} \mathbf{M} \times (\mathbf{M} \times (\frac{2A}{M_s} \nabla^2 \mathbf{b} + \mathbf{H}_d + \mathbf{H}_a + \mathbf{H}_{\text{anis}})) \end{aligned} \quad (5.0.9)$$

a modified Landau-Lifshitz-Gilbert equation of motion that describes the dynamic magnetization process in a given sample.

In the equation above the precession and the damping term are governed not only by the contributing fields and intrinsic properties of the sample but also by the phenomenological Gilbert damping constant α . The Gilbert damping term includes all the damping forces of a system. Damping involves loss of energy from macroscopic motion of the local magnetization field by transfer of energy to microscopic thermal motion. There are different kind of mechanisms involved such as coupling of the magnetization field to spin waves, lattice vibrations, effects of polycrystalline structure,

strains, crystal defects and eddy currents. Especially in high conductivity materials $\sigma > 10^5(\Omega m)^{-1}$ and high frequency fields the contribution of eddy currents become more important. In the following chapter a theory will be presented to extract the eddy current contribution from the damping term.

Chapter 6

Eddy Currents

Since 1955, a number of different damping mechanisms had been studied [15]-[38] and the results have shown that the damping mechanism is very complex and different for each material, but for metallic ferromagnets it was found that eddy currents are the dominant mechanism.

The rate of magnetization and remagnetization in ferromagnetic materials is governed by damping mechanisms. Damping is about transfer of loss of energy from the macroscopic motion of the local magnetization field to the microscopic thermal motion. It should be mentioned that the local magnetization field $\mathbf{M}(\mathbf{r})$ is the expectation value of the magnetic moment per unit volume due to spins and orbital motion of unpaired electrons averaged over a few lattice cells. The orbital motion is not discussed in detail, it is rather included by adjusting the gyromagnetic ratio (see chapter 3).

The mechanisms by which the energy transfer occurs include the coupling of the magnetization field to spin waves, lattice vibrations, the effects of polycrystalline structure, strains, crystal effects such as voids and foreign atoms, and eddy currents. So far eddy current effects are usually not taken into account in standard magnetic calculations, that are based on assumptions of quasistatic approximation, small material conductivity or that the contribution of eddy currents is included in the dimensionless

damping constant of the Landau-Lifshitz-Gilbert equation.

The main motivation to develop a dynamic micromagnetic model that includes eddy currents is the importance of accurate calculations of time dependent micromagnetic processes for magnetic data storage (hard disk recording magnetic, random access memory MRAM) at high data rates and the demand for ultrafast switching in magnetic nanostructures. Especially for magnetic recording heads with field rise times of less than 0.1 ns and a high conductivity σ of $0.6 \cdot 10^7 (\Omega m)^{-1}$, the assumptions above are no longer applicable.

Several eddy current methods have been presented in the past. These include the two-dimensional quasistatic model by Della Torre and Eicke [39] and the one-dimensional dynamic calculation by Sandler and Bertram [40]. A hybrid method for three-dimensional eddy current problems that is based on the solution of the differential equation for the current density and the magnetic field where the Bio-Savart law is used to calculate the field intensity of the magnetic field on the surface was introduced by Kalimov and co-workers [41]. Serpico and co-workers [42] developed a finite difference scheme that is applied to the analysis of eddy currents with the Landau-Lifshitz equation as a constitutive relation.

We developed a three-dimensional finite element dynamic micromagnetic model including eddy currents. Our model simultaneously solves the Landau-Lifshitz-Gilbert (LLG) equation and the quasistatic Maxwell equation using a hybrid finite element/boundary element (FE/BE) method. A FE method with a linear basis function is used to discretize the conducting region Ω . To calculate the magnetization vector on each node of our mesh a Voronoi tessellation was used to calculate the exact volume around each node. The boundary element method is used to map the boundary conditions of the magnetic field at infinity on equivalent boundary conditions on the surface of the conducting region Ω , which reduces the necessity of a mesh to Ω . The eddy current field is introduced as an additional part of the effective magnetic field

in the LLG equation, and is directly calculated from the space time behavior of the magnetization rate of change.

6.1 Eddy Current Model

To formulate the eddy current model we consider a conducting region Ω with the conductivity σ and the magnetic permeability μ . Eddy currents are induced inside the region by applying an external magnetic field which changes the magnetization. The dynamic magnetization process in the conducting region is described by the LLG equation of motion

$$\frac{\partial \mathbf{M}}{\partial t} = -\dot{\gamma}_0 \mathbf{M} \times \mathbf{H}_{\text{eff}} - \frac{\alpha \dot{\gamma}_0}{M_s} \mathbf{M} \times (\mathbf{M} \times \mathbf{H}_{\text{eff}}) \quad (6.1.1)$$

where

$$\dot{\gamma}_0 = \frac{\gamma_0}{1 + \alpha^2} \quad (6.1.2)$$

and α is a dimensionless damping constant (the modified Gilbert damping constant without the eddy current damping effects) and γ_0 is the electron gyromagnetic ratio. The effective field \mathbf{H}_{eff} is composed of the anisotropy field \mathbf{H}_{anis} , the exchange contributions \mathbf{H}_{exch} , the applied field \mathbf{H}_a , the magnetostatic field \mathbf{H}_d and to take care of eddy current effects an eddy current field \mathbf{H}_{eddy} is introduced:

$$\mathbf{H}_{\text{eff}} = \mathbf{H}_{\text{anis}} + \mathbf{H}_{\text{exch}} + \mathbf{H}_a + \mathbf{H}_d + \mathbf{H}_{\text{eddy}} \quad (6.1.3)$$

6.1.1 Eddy Current Diffusion Equation

To derive the conditional equations for the eddy current field one starts with the Maxwell equations. In electromagnetics we have the electric and magnetic fields \mathbf{E}, \mathbf{H} , the electric and magnetic flux densities \mathbf{D}, \mathbf{B} , and the constitutive relations

$$\mathbf{D} = \epsilon \mathbf{E} \quad (6.1.4)$$

$$\mathbf{B} = \mu \mathbf{H} \quad (6.1.5)$$

where ϵ is the permittivity, μ the magnetic permeability which is defined

$$\mu = (1 + \chi_m)\mu_0 \quad (6.1.6)$$

with μ_0 being the permeability of free space and χ_m the magnetic susceptibility.

Writing here the Maxwells Equations in terms of \mathbf{E} and \mathbf{B} ,

$$\epsilon \frac{\partial \mathbf{E}}{\partial t} = \nabla \times \frac{1}{\mu} \mathbf{B} - \sigma \mathbf{E} - \mathbf{j}_s \quad (6.1.7)$$

$$\frac{\partial \mathbf{B}}{\partial t} = -\nabla \times \mathbf{E} \quad (6.1.8)$$

$$\nabla \cdot \epsilon \mathbf{E} = 0 \quad (6.1.9)$$

$$\nabla \cdot \mathbf{B} = 0 \quad (6.1.10)$$

with appropriate boundary conditions and initial conditions understood. Notifying that \mathbf{j}_s is an independent current source term depending on the problem it may or may not be added. In the following definition all the material parameters ϵ , μ , σ are free to be symmetric positive definite tensor functions of space, but as we impose the restriction that they should be independent of time.

In the following we consider to solve the Maxwells Equations for a good conductor, which is defined by the condition

$$\epsilon \frac{\partial \mathbf{E}}{\partial t} \ll \sigma \mathbf{E}. \quad (6.1.11)$$

Equation 6.1.11 depends not only on the material parameters σ and ϵ , but also on the time rate of change of the electric field \mathbf{E} . Taking 6.1.11 into account, Maxwells equations can be simplified by neglecting the displacement current $\epsilon \frac{\partial \mathbf{E}}{\partial t}$ altogether. This is called the low-frequency approximation, diffusion approximation or eddy current approximation. A detailed mathematical analysis which gives a justification to the approximation is given in [43].

The modified Maxwells equations with the constitutive relations are defined as follows

$$\nabla \times \frac{1}{\mu} \mathbf{B} = \sigma \mathbf{E} + \mathbf{j}_s \quad (6.1.12)$$

$$\frac{\partial \mathbf{B}}{\partial t} = -\nabla \times \mathbf{E} \quad (6.1.13)$$

$$\nabla \cdot \epsilon \mathbf{E} = 0 \quad (6.1.14)$$

$$\nabla \cdot \mathbf{B} = 0 \quad (6.1.15)$$

with $\mathbf{B} = \mu_0(\mathbf{H} + \mathbf{M})$. The equation 6.1.12 and 6.1.15 are recast to

$$\nabla \times \mu_0(\mathbf{H} + \mathbf{M}) = \mu_0(1 + \chi_m)\sigma \mathbf{E} + \mathbf{j}_s \quad (6.1.16)$$

$$\nabla \cdot \mu_0(\mathbf{H} + \mathbf{M}) = 0 \quad (6.1.17)$$

and by neglecting \mathbf{j}_s and splitting the the current $\sigma \mathbf{E} = \mathbf{j}$ in two components

$$\mathbf{j} = \mathbf{j}_{\text{free}} + \mathbf{j}_{\text{mat}} \quad (6.1.18)$$

with \mathbf{j}_{free} being free currents and \mathbf{j}_{mat} being material currents the following equation is derived

$$\nabla \times \mu_0(\mathbf{H} + \mathbf{M}) = \mu_0(\mathbf{j}_{\text{free}} + \mathbf{j}_{\text{mat}}). \quad (6.1.19)$$

Material currents and the magnetization are connected through the following identity

$$\nabla \times \mathbf{M} = \mathbf{j}_{\text{mat}} = \chi_m \sigma \mathbf{E} \quad (6.1.20)$$

if applied to the equations above the following condition equations are derived

$$\nabla \times \mathbf{H} = \sigma \mathbf{E} \quad (6.1.21)$$

$$\nabla \cdot \mathbf{H} = -\nabla \cdot \mathbf{M} \quad (6.1.22)$$

By splitting the field $\mathbf{H} = \mathbf{H}_d + \mathbf{H}_{\text{eddy}}$ into two parts, in an irrotational field and in a solenoidal field, two set of equations with different source terms are obtained. As the source of the eddy current field is a current induced in the sample similar to the

applied field, it can be treated as a solenoidal field. Therefore the resulting conditional Maxwell equations are

$$\nabla \cdot \mathbf{H}_{\text{eddy}} = 0 \quad (6.1.23)$$

$$\nabla \times \mathbf{H}_{\text{eddy}} = \mathbf{j}_{\text{eddy}} \quad (6.1.24)$$

with \mathbf{j}_{eddy} being the eddy current source term. To calculate the eddy current field the curl operator is applied on equation 6.1.24

$$\nabla \times (\nabla \times \mathbf{H}_{\text{eddy}}) = \nabla \times \mathbf{j}_{\text{eddy}} \quad (6.1.25)$$

The term $\nabla \times \nabla \times$ is recast by using the following vector identity

$$\nabla \times \nabla \times = \nabla(\nabla \cdot) - \nabla \cdot (\nabla) \quad (6.1.26)$$

and equation 6.1.25 is rewritten to

$$\nabla(\nabla \cdot \mathbf{H}_{\text{eddy}}) - \nabla \cdot (\nabla \mathbf{H}_{\text{eddy}}) = \nabla \times \mathbf{j}_{\text{eddy}} \quad (6.1.27)$$

As defined above, the divergence of the eddy current field \mathbf{H}_{eddy} is equal to zero meaning that the first term in 6.1.27 vanishes. The current is recast in terms of the electric field

$$\mathbf{j}_{\text{eddy}} = \sigma \mathbf{E} \quad (6.1.28)$$

and introduced in 6.1.27

$$-\nabla^2 \mathbf{H}_{\text{eddy}} = -\Delta \mathbf{H}_{\text{eddy}} = \nabla \times (\sigma \mathbf{E}) \quad (6.1.29)$$

Applying Faradays law in differential form

$$\nabla \times \mathbf{E} = -\frac{\partial \mathbf{B}}{\partial t} \quad (6.1.30)$$

and 6.1.3 to 6.1.29 yields

$$-\Delta \mathbf{H}_{\text{eddy}} = -\sigma \mu_0 \left(\frac{\partial \mathbf{H}_a}{\partial t} + \frac{\partial \mathbf{H}_d}{\partial t} + \frac{\partial \mathbf{H}_{\text{eddy}}}{\partial t} + \frac{\partial \mathbf{M}}{\partial t} \right) \quad (6.1.31)$$

Considering that for soft magnetic materials the change of the applied and the magnetostatic field over time is much smaller than the magnetization [44] a diffusion equation for the eddy current field is derived

$$\Delta \mathbf{H}_{\text{eddy}} - \sigma \mu_0 \frac{\partial \mathbf{H}_{\text{eddy}}}{\partial t} = \sigma \mu_0 \frac{\partial \mathbf{M}}{\partial t} \quad (6.1.32)$$

This equation is true everywhere in space but has to be adjusted for the material components for the different regions of interest.

The Poisson equation 6.1.32 for the eddy current field inside and outside of the conducting region is

$$\Delta \mathbf{H}_{\text{eddy}} = \begin{cases} \sigma \mu_0 \frac{\partial \mathbf{H}_{\text{eddy}}}{\partial t} + \sigma \mu_0 \frac{\partial \mathbf{M}}{\partial t} & \Omega \\ 0 & \mathbb{R}^3 \setminus \Omega \end{cases} \quad (6.1.33)$$

with the boundary condition at infinity, $\mathbf{H}_{\text{eddy}} = 0$. To solve the partial differential equation and to derive a unique solution, appropriate boundary conditions for the eddy current field have to be found.

6.1.2 Boundary Conditions

The tangential component of the boundary condition on the surface of the conducting region $\partial\Omega$ is

$$\mathbf{n} \times \mathbf{H}_{\text{eddy}}^{\text{in}} - \mathbf{n} \times \mathbf{H}_{\text{eddy}}^{\text{out}} = 0. \quad (6.1.34)$$

where \mathbf{n} is the unit vector pointing outward from Ω . Another boundary condition is on the normal derivative of the eddy current field \mathbf{H}_{eddy} . It is derived by starting with equation 6.1.29 and expanding the derivatives of $\sigma \mathbf{E}$

$$\nabla \times (\nabla \times \mathbf{H}_{\text{eddy}}) = \sigma \nabla \times \mathbf{E} + \nabla \sigma \times \mathbf{E} \quad (6.1.35)$$

a term is gained in $\nabla \sigma$. The conductivity is piecewise constant, which means that this term vanishes inside and outside of Ω . However, $\nabla \sigma$ is singular at the boundary

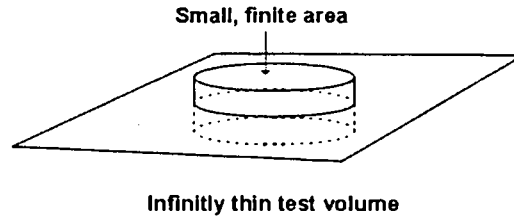


Figure 6.1: Infinitely thin test volume $\hat{\Omega}$ on the boundary $\partial\Omega$.

where σ has a jump discontinuity and this puts a surface load (delta function) to the right-hand side of 6.1.30. Because of the second derivatives on the left-hand side, the net result is that the normal derivative of \mathbf{H}_{eddy} is discontinuous at the boundary. To calculate the jump discontinuity, equation 6.1.27 is integrated over an infinitely thin test volume $\hat{\Omega}$ straddling a small portion of the boundary $\partial\Omega$ see Fig.6.1,

$$\int_{\hat{\Omega}} \Delta \mathbf{H}_{\text{eddy}} dV = - \int_{\hat{\Omega}} \nabla \times \mathbf{j}_{\text{eddy}} dV. \quad (6.1.36)$$

Taking the equation above and applying Gauss's theorem, which is defined as follows

$$\int_V \nabla \cdot \mathbf{F} dV = \int_S \mathbf{F} \cdot \mathbf{n} da \quad (6.1.37)$$

with \mathbf{F} being a vector field, V the volume and S a given enclosed surface with an outward pointing unit normal \mathbf{n} , to convert 6.1.36 into an integral over the boundary $\partial\hat{\Omega}$,

$$\int_{\partial\hat{\Omega}} (da \mathbf{n} \cdot \nabla) \mathbf{H}_{\text{eddy}} = - \int_{\partial\hat{\Omega}} da \mathbf{n} \times \mathbf{j}_{\text{eddy}}. \quad (6.1.38)$$

The dominant contributions come from two surfaces parallel to the conducting surface $\partial\Omega$, just inside and just outside Ω , with unit normals da along $-\mathbf{n}$ and $+\mathbf{n}$, respectively. Thence equation 6.1.38 is converted to a surface integral over $\hat{\Omega} \cap \partial\Omega$ that involves the differences between the two sides of $\partial\Omega$. Since the test volume $\hat{\Omega}$ is arbitrary, the integrand must vanish identically on the surface $\partial\Omega$. Furthermore since \mathbf{j}_{eddy} exists only inside the conducting region and is zero outside of Ω the following

expression for the boundary condition is derived

$$(\mathbf{n} \cdot \nabla) \mathbf{H}_{\text{eddy}}^{\text{in}} - (\mathbf{n} \cdot \nabla) \mathbf{H}_{\text{eddy}}^{\text{out}} = -\mathbf{n} \times \mathbf{j}_{\text{eddy}} \quad (6.1.39)$$

6.2 Calculation of the Eddy Current Field

In the previous section a diffusion equation for the eddy current field for the whole region \mathbb{R}^3

$$-\Delta \mathbf{H}_{\text{eddy}} = -\sigma \mu_0 \left(\frac{\partial \mathbf{H}_a}{\partial t} + \frac{\partial \mathbf{H}_d}{\partial t} + \frac{\partial \mathbf{H}_{\text{eddy}}}{\partial t} + \frac{\partial \mathbf{M}}{\partial t} \right) \quad (6.2.1)$$

and the governing boundary conditions

$$\mathbf{n} \times \mathbf{H}_{\text{eddy}}^{\text{in}} = \mathbf{n} \times \mathbf{H}_{\text{eddy}}^{\text{out}} \quad (6.2.2)$$

$$(\mathbf{n} \cdot \nabla) \mathbf{H}_{\text{eddy}}^{\text{in}} - (\mathbf{n} \cdot \nabla) \mathbf{H}_{\text{eddy}}^{\text{out}} = -\mathbf{n} \times \mathbf{j}_{\text{eddy}} \quad (6.2.3)$$

at the interface between the conducting region Ω and $\mathbb{R}^3 \setminus \Omega$ are derived. To find a solution, the diffusion equation is treated like any other normal partial differential equation.

The Poisson equation 6.2.1 is solved by taking advantage of the linearity of 6.1.33 and the solution is split into two parts

$$\mathbf{H}_{\text{eddy}} = \mathbf{H}_{\text{eddy}}^1 + \mathbf{H}_{\text{eddy}}^2 \quad (6.2.4)$$

with $\mathbf{H}_{\text{eddy}}^1$ being the solution of the inhomogeneous and $\mathbf{H}_{\text{eddy}}^2$ the homogeneous part of the partial differential equation. Defining the contributions of the solutions to the separate regions of the problem

$$\mathbf{H}_{\text{eddy}} = \begin{cases} \mathbf{H}_{\text{eddy}}^2 + \mathbf{H}_{\text{eddy}}^1 & \text{in } \Omega \\ \mathbf{H}_{\text{eddy}}^2 & \text{in } \mathbb{R}^3 \setminus \Omega \end{cases} \quad (6.2.5)$$

it is found that $\mathbf{H}_{\text{eddy}}^1$ is zero outside of Ω .

eddy current field inside of Ω

$\mathbf{H}_{\text{eddy}}^1$ is the particular solution that solves the following inhomogeneous boundary problem

$$\Delta \mathbf{H}_{\text{eddy}}^1 = \sigma \mu_0 \frac{\partial \mathbf{H}_{\text{eddy}}^1}{\partial t} + \sigma \mu_0 \frac{\partial \mathbf{H}_{\text{eddy}}^2}{\partial t} + \sigma \mu_0 \frac{\partial \mathbf{M}}{\partial t} \quad (6.2.6)$$

The appropriate boundary condition needed to solve 6.2.6 for $\mathbf{H}_{\text{eddy}}^1$ on the surface $\partial\Omega$ of the conducting region is

$$(\mathbf{n} \cdot \nabla) \mathbf{H}_{\text{eddy}}^1 = -\mathbf{n} \times \mathbf{j}_{\text{eddy}}. \quad (6.2.7)$$

with the current term \mathbf{j}_{eddy} , which is substituted by the curl of the eddy current field $\nabla \times \mathbf{H}_{\text{eddy}}^1$.

eddy current field outside of Ω

$\mathbf{H}_{\text{eddy}}^2$ is the homogeneous particular solution of the eddy current diffusion equation. It is a solution of the Laplace equation

$$\Delta \mathbf{H}_{\text{eddy}}^2 = 0 \quad (6.2.8)$$

with the following boundary conditions

$$\mathbf{H}_{\text{eddy}}^{2;\text{out}} - \mathbf{H}_{\text{eddy}}^{2;\text{in}} = \mathbf{H}_{\text{eddy}}^{1;\text{in}} \quad (6.2.9)$$

which puts the constrain on the solution that the eddy field inside is the same as the eddy field outside, and

$$(\mathbf{n} \cdot \nabla) \mathbf{H}_{\text{eddy}}^{2;\text{out}} - (\mathbf{n} \cdot \nabla) \mathbf{H}_{\text{eddy}}^{2;\text{in}} = 0 \quad (6.2.10)$$

that the normal derivative of each component of the eddy current field inside of Ω is equal to the normal derivative of each component of the eddy current field outside. From 6.2.8 to 6.2.10 it can be deduced that the components of $\mathbf{H}_{\text{eddy}}^2$ can be written

in analogy to the potential solution of a magnetic dipole sheet.

$$\mathbf{H}_{\text{eddy}}^2 = \int_{\partial\Omega} \mathbf{H}_{\text{eddy}}^{2;\text{out}} \mathbf{n} \cdot \nabla \left(\frac{1}{|\mathbf{r} - \mathbf{r}'|} \right) da - \int_{\partial\Omega} \mathbf{H}_{\text{eddy}}^{2;\text{in}} \mathbf{n} \cdot \nabla \left(\frac{1}{|\mathbf{r} - \mathbf{r}'|} \right) da + \left(\frac{\Theta(\mathbf{r})}{4\pi} - 1 \right) (\mathbf{H}_{\text{eddy}}^{2;\text{out}} - \mathbf{H}_{\text{eddy}}^{2;\text{in}}) \quad (6.2.11)$$

with the boundary condition 6.2.10 it can be recast to

$$\mathbf{H}_{\text{eddy}}^2 = \int_{\partial\Omega} \mathbf{H}_{\text{eddy}}^1 \mathbf{n} \cdot \nabla \left(\frac{1}{|\mathbf{r} - \mathbf{r}'|} \right) da + \left(\frac{\Theta(\mathbf{r})}{4\pi} - 1 \right) \mathbf{H}_{\text{eddy}}^1 \quad (6.2.12)$$

where $\Theta(\mathbf{r})$ is the solid angle subtended by $\partial\Omega$ at \mathbf{r} .

The final solution of the eddy current field is composed of the homogeneous and the inhomogeneous solution of the eddy current diffusion equation.

The equations 6.1.1 to 6.2.10 are a coupled system of Landau–Lifshitz–Gilbert and quasi-static Maxwell equations that is solved by a hybrid finite element/boundary element (FE/BE) method. For the region Ω a finite element method with the Galerkin weak formulation is used. For the non-conducting region $\mathbb{R}^3 \setminus \Omega$ a boundary element (BE) method is used to map the boundary conditions (BC) of the magnetic field at infinity on equivalent BC on the surface of Ω as presented by Fredkin and Koehler [45].

Chapter 7

Numerical Technique and Algorithm

In this chapter the numerical method and algorithm used to solve the coupled system of Landau–Lifshitz–Gilbert and quasi-static Maxwell equations 6.1.1 to 6.1.32 is presented. A set of three equations, two differential equations, the Landau–Lifshitz–Gilbert equation of motion

$$\frac{\partial \mathbf{M}}{\partial t} = -\frac{\gamma_0}{1 + \alpha^2} \mathbf{M} \times \mathbf{H}_{\text{eff}} - \frac{\alpha \gamma_0}{M_s(1 + \alpha^2)} \mathbf{M} \times (\mathbf{M} \times \mathbf{H}_{\text{eff}}) \quad (7.0.1)$$

and the eddy current diffusion equation for the $\mathbf{H}_{\text{eddy}}^1$ field,

$$\Delta \mathbf{H}_{\text{eddy}}^1 = \sigma \mu_0 \frac{\partial \mathbf{H}_{\text{eddy}}^1}{\partial t} + \sigma \mu_0 \frac{\partial \mathbf{H}_{\text{eddy}}^2}{\partial t} + \sigma \mu_0 \frac{\partial \mathbf{M}}{\partial t} \quad (7.0.2)$$

and one algebraic equation, the Laplace equation for $\mathbf{H}_{\text{eddy}}^2$,

$$\Delta \mathbf{H}_{\text{eddy}}^2 = 0 \quad (7.0.3)$$

has to be solved. In addition two further equations governing the demagnetization field are solved. This set of differential and algebraic equations (DAEs) is an initial value problem and is solved using an implicit differential-algebraic (IDA) solver. The

initial value problem is integrated using a backward differentiation formula (BDF) method implemented in a variable-order, variable-step form. Applying the BDF on the DAE system results in a nonlinear algebraic system that is solved with a Newton iteration. This leads to a linear system for each Newton correction that is solved with a scaled preconditioned generalized minimum residual (SPGMR) method [46].

7.1 Implicit Differential Algebraic Solver

IDA is a general purpose solver for the initial value problem for systems of differential algebraic equations (DAEs). The implicit differential algebraic solver is based on DASPK [47], [48] and in the solution of the underlying nonlinear system uses an inexact Newton/Krylov (iterative) rather than the Newton/direct method at each time step. The Newton/Krylov method uses the generalized minimal residual (GMRES) linear iterative method [49], and compared to direct methods requires almost no matrix storage for solving the Newton equations.

IDA solves the initial value problem for the DAE system in the general form

$$F(t, \mathbf{y}, \dot{\mathbf{y}}) = 0 \quad (7.1.1)$$

where \mathbf{y} and F are vectors in \mathbb{R}^N (in our case $N = 9J$) of the form

$$\mathbf{y}_j = \mathbf{y}_j \begin{pmatrix} \mathbf{b} \\ \mathbf{H}_{\text{eddy}}^1 \\ \mathbf{H}_{\text{eddy}}^2 \end{pmatrix} \quad \mathbf{b}, \mathbf{H}_{\text{eddy}}^1, \mathbf{H}_{\text{eddy}}^2 \in \mathbb{R}^3 \quad (7.1.2)$$

with t being the time and j is the node index with values from 1 to J . The initial conditions

$$\mathbf{y}(t_0) = \mathbf{y}_0, \quad \dot{\mathbf{y}}(t_0) = \dot{\mathbf{y}}_0 \quad (7.1.3)$$

given. The initial vectors \mathbf{y}_0 and $\dot{\mathbf{y}}_0$ are not arbitrary and must be consistent with 7.1.1.

The implicit differential solver integrates the system 7.1.1 with backward differentiation formula (BDF) methods which are implemented in a variable-order, variable-step form. The method orders range from 1 to 5 and the BDF of order k is given by the following multistep equation

$$\sum_{i=0}^k \alpha_{n,i} \mathbf{y}_{n-i} = h_n \dot{\mathbf{y}}_n \quad (7.1.4)$$

with \mathbf{y}_n and $\dot{\mathbf{y}}_n$ being the computed approximations to $\mathbf{y}_n(t_n)$ and $\dot{\mathbf{y}}_n(t_n)$, respectively, and the step-size h_n is

$$h_n = t_n - t_{n-1}. \quad (7.1.5)$$

$\alpha_{n,i}$ are coefficients that are uniquely determined by the order k and the step-size history. Applying the backward differential formula method to the differential algebraic system 7.1.1 results in a nonlinear algebraic system which has to be solved at each step

$$\mathbf{G}(\mathbf{y}_n) = \mathbf{F}(t_n, \mathbf{y}_n, h_n^{-1} \sum_{i=0}^k \alpha_{n,i} \mathbf{y}_{n-i}) = 0 \quad (7.1.6)$$

The nonlinear system 7.1.6 is solved using a Newton iteration, which leads to a linear system for each Newton correction of the form

$$\mathbf{J}[\mathbf{y}_{n(m+1)} - \mathbf{y}_{n(m)}] = -\mathbf{G}(\mathbf{y}_{n(m)}) \quad (7.1.7)$$

where $\mathbf{y}_{n(m)}$ is the m^{th} approximation to \mathbf{y}_n and \mathbf{J} is an approximation of systems Jacobian

$$\mathbf{J} = \frac{\partial \mathbf{G}}{\partial \mathbf{y}} = \frac{\partial \mathbf{F}}{\partial \mathbf{y}} + \alpha \frac{\partial \mathbf{F}}{\partial \dot{\mathbf{y}}} \quad (7.1.8)$$

where $\alpha = \alpha_{n,0}/h_n$, and it changes whenever the step size changes or the method order.

An iterative method is used to calculate the solution of the approximated Jacobian 7.1.7, namely, the scaled preconditioned GMRES, denoted SPGMR.

The equation 7.1.7 is written abstractly as

$$Ax = b \quad (7.1.9)$$

and to solve it, a preconditioned matrix P is sought that approximates A , with an easy to solve linear form of

$$Px = b. \quad (7.1.10)$$

The preconditioning matrix P is obtained by using an incomplete LU factorization (ILU), where

$$P = LU \quad (7.1.11)$$

and LU is obtained from a Gauss elimination procedure. Preconditioning is applied to the left side of 7.1.9 and scaling is introduced by a diagonal scaling matrix D , with the weights w^i as diagonal elements. Thus the system that is solved with the GMRES method is

$$(D^{-1}P^{-1}AD)(D^{-1}x) = D^{-1}P^{-1}b \quad (7.1.12)$$

or

$$\bar{A}\bar{x} = \bar{b}. \quad (7.1.13)$$

7.1.1 Error control

While integrating, the system estimates a mean norm E_n of the local truncation error at the n^{th} time step, that has to satisfy the inequality

$$\|E_n\|_{wrms} < 1 \quad (7.1.14)$$

and imposes a tolerance on the local errors by way of the weighted root mean square (wrms) norm, defined as

$$\|E_n\| = \left[\frac{1}{N} \sum_{i=1}^N \left(\frac{E_n^i}{w^i} \right)^2 \right]^{\frac{1}{2}} \quad (7.1.15)$$

with the superscript i denoting the i^{th} component and w^i the i^{th} weight

$$w^i = \text{rtol}|y^i| + \text{atol} \quad \text{or} \quad w^i = \text{rtol}|y^i| + \text{atol}. \quad (7.1.16)$$

The scalar relative error tolerance (rtol) and the absolute error tolerance (atol) permit to define an allowed error per step and thus a control of the magnitude of the error.

Chapter 8

Eddy Current and Magnetization

In the recent years the increasing demand for ultra-fast switching in magnetic nanostructures lead to more accurate models for high-speed switching in conducting ferromagnetic materials. It is apparent that eddy currents which are induced by high frequency fields with rise times of < 0.1 ns effect the magnetic behavior of conducting ferromagnetic materials.

Several models treating different kind of problems were developed. Mayergoyz et al. [50] presented a self-consistent numerical solution of the magnetic diffusion equation and the Landau-Lifshitz equation for linearly and circularly polarized applied magnetic fields and showed the effect of eddy currents for different conducting ferromagnetic films. L. Torres et al. [51] developed a 3-dimensional micromagnetic model that included eddy currents and investigated the magnetization behavior for high conductivity materials.

To understand the influence of eddy current contributions on magnetic nano-scale structures, the very basic mechanism that governs the magnetization process has to be investigated.

In the last chapters the theory to describe the magnetization processes of magnetic structures, a 3-dimensional finite element/boundary element model that includes eddy

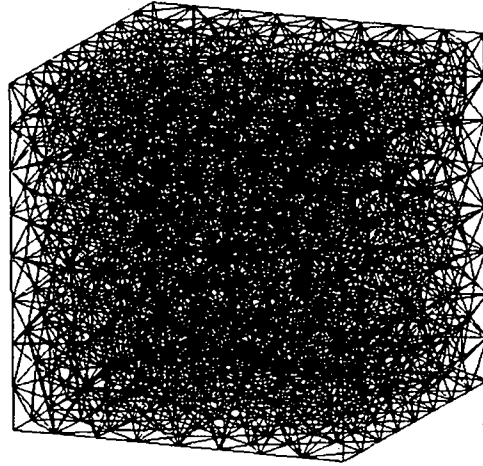


Figure 8.1: Domain of interest discretized with tetrahedral basis-functions.

current effects, was developed. It will be used to investigate in detail the effect of eddy currents (here the eddy current field) on the magnetization reversal of cubic single domain particles.

8.1 Finite Element Discretization

To be able to simulate the magnetization motion of the magnetic moments the conducting region is discretized with the finite element method with linear basis functions, see Fig. 8.1. On every node of the discretized region is a magnetization vector, for whom the equation of magnetization motion is solved.

The magnetization \mathbf{M} of a system can be expressed in terms of a magnetization \mathbf{m} per unit volume V .

$$\mathbf{M} = \frac{\mathbf{m}}{V} \quad (8.1.1)$$

To calculate the magnetization vector on each node of our mesh an additional discretization was used to calculate the exact volume around each node. First a Delaunay

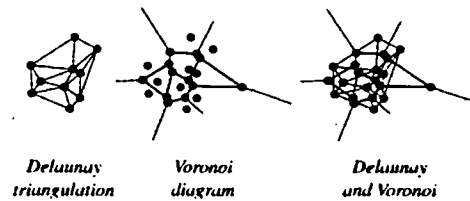


Figure 8.2: Delaunay–Triangulation.

triangulation, which is the triangulation with empty circumferences, is calculated by computing a convex hull. The triangulation lifts the input sites to a paraboloid by adding the sum of the squares of the coordinates. It computes the convex hull of the lifted sites, and projects the lower convex hull to the input. Each region of the Delaunay triangulation corresponds to a facet of the lower half of the convex hull. Facets of the upper half of the convex hull correspond to the furthest-site Delaunay triangulation. Once the triangulation is finished the Voronoi diagrams are calculated. And with the Voronoi points a convex volume around each node is constructed, see Fig. 8.2.

The volume of the voronoi diagram gives a partition of the total volume, with mutually distinct volumes surrounding each node of the finite element mesh. This volume is used to define a magnetic moment and the effective field at each node point [52]. Given the magnetic field and the effective field for each node point, the LLG equations becomes a system of ordinary differential equations. To summarize the discretization scheme is as follows:

1. Linear finite elements are used to discretize Gibbs energy as a function of the magnetization
2. The magnetostatic boundary value problem for the magnetic potential and the eddy current diffusion equation are solved using standard finite element techniques

3. A magnetic moment and the corresponding effective field are defined at each node of the finite element grid using the voronoi partition
4. The resulting differential algebraic system of equation is solved using an implicit time integration scheme.

8.2 Precession and Damping Term

The behavior of magnetic moments in magnetic structures is described as presented earlier by the Landau–Lifshitz–Gilbert equation. The motion of the magnetic spins is composed of a precession and a dampened motion, presented by the precession term and the damping term, respectively.

To analyze these two terms in detail, a permalloy nanocube with an edge length of 27nm and 1195 nodes was discretized into 5649 tetrahedrons with 862 surface elements. The nanocube is initially magnetized uniformly in positive z-direction and exposed to an external field of $\mathbf{B}_{ext} = \mu_0 \mathbf{H}_{ext} = -100 \mathbf{u}_z mT$. The LLG equation is solved for the nanocube with two different damping values. Investigated is the path of the magnetization vector over time, see Fig. 8.3, with a high damping of $\alpha = 1$, see Fig. 8.4, and with a low damping of $\alpha = 0.1$, see Fig. 8.5.

From the figures 8.4 and 8.5 the influence of the damping parameter on the precession as well as on the damping term, and therefor on the whole magnetization reversal time can be deduced. The major difference, considered from the magnetization reversal, is that for a high damping the precession of the magnetization vector is minimized and the damping motion is maximized, resulting, for a given applied field, in a fast magnetization reversal. For low damping, the precession motion is the dominant factor in the magnetization reversal.

Hence, the minimum magnetization reversal time occurs when

$$\alpha_{min} = 1 \tag{8.2.1}$$

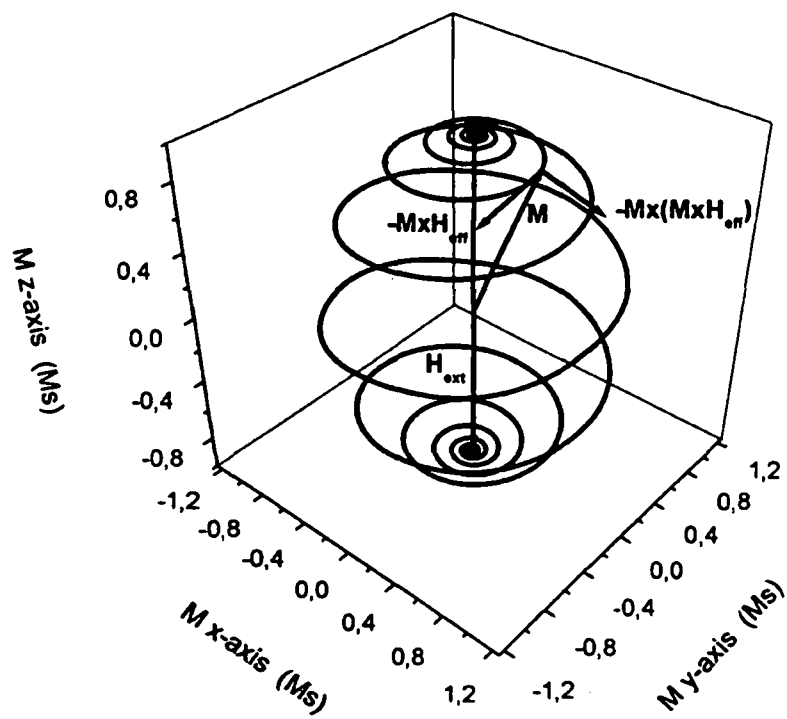


Figure 8.3: Trajectory of the Magnetization Vector over time.

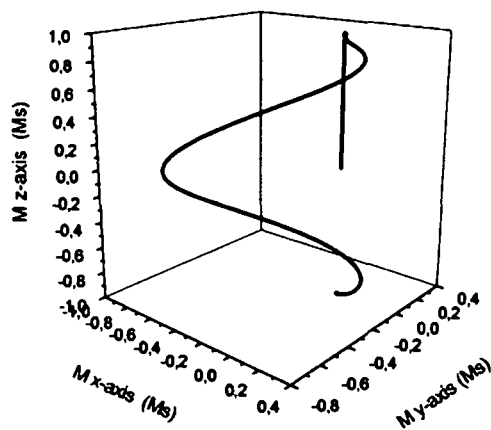


Figure 8.4: Trajectory of the Magnetization Vector over time, for high damping.

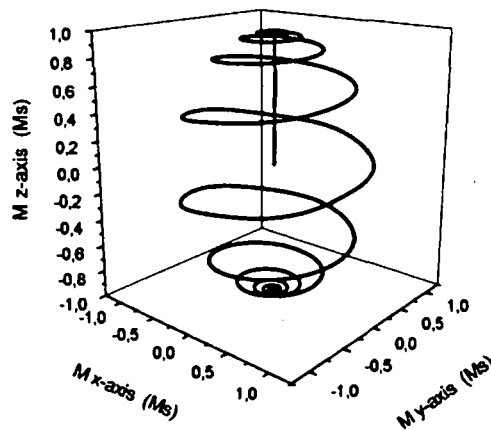


Figure 8.5: Trajectory of the Magnetization Vector over time, for low damping.

Table 8.1: Magnetization reversal results for a 27 nm cube in an applied field of $\mathbf{H}_{\text{ext}} = -800\mathbf{u}_z mT$ with α values ranging from 1 to 0.005. M_z^1 gives the time for the magnetization to reach the xy-plane in units of ns, and M_z^2 gives the time for the magnetization to reach $-0.99 M_s$ in units of ns.

α	M_z^1	M_z^2
1.0	0.180	0.219
0.5	0.207	0.255
0.2	0.278	0.376
0.1	0.415	0.567
0.08	0.483	0.664
0.06	0.564	0.810
0.04	0.569	0.947
0.02	0.614	1.173
0.01	0.592	1.646
0.005	0.831	2.148

which is consistent with analytical results obtained by Ryoichi Kikuchi [53]. For $\alpha < 1$, the magnetization vector \mathbf{M} moves faster, but rotates around the external magnetic field so that the net travelling time between the initial and the final state becomes longer.

8.2.1 Magnetization Reversal

To derive the magnetization reversal time in dependency of the damping constant α , simulations were performed for an 27nm cube under the influence of an applied field of $\mathbf{H}_{\text{ext}} = -800\mathbf{u}_z mT$ with different values for α , see Table 8.1. The magnetization reversal curves of the magnetization vector in z-direction from its initial state in +z-direction to its final state in -z-direction were investigated and the reversal time was recorded at two spots of the magnetization reversal. M_z^1 gives the reversal time values of the magnetization vector while it is lying in the x-y plane and M_z^2 gives the

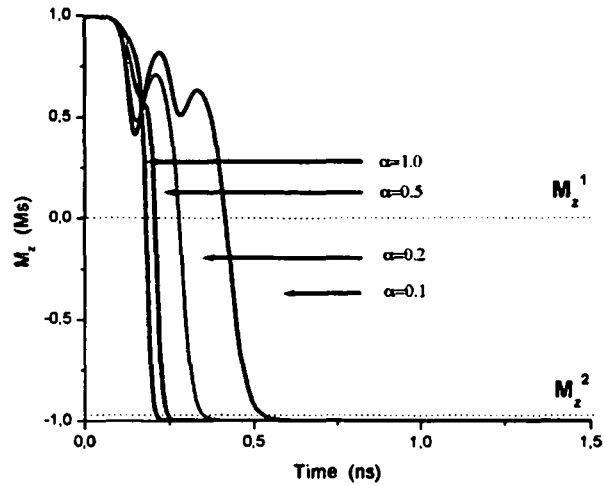


Figure 8.6: Magnetization reversal as a function of Damping constant α versus time (ns), for $\alpha = 1, 0.5, 0.2, 0.1$.

magnetization reversal time shortly before the magnetization reversal is complete, see Figures 8.6 to 8.8 and Table 8.1 for the calculated values. By decreasing the damping constant the magnetization vector starts to precess around the external field which takes it longer to reach its final equilibrium condition. The values of M_z^1 and M_z^2 were plotted over time in Fig. 8.9 to derive a correlated behavior of the magnetization reversal time and the damping-constant. The Figures 8.6 to 8.8 show that the reversal time and the value of the Gilbert damping constant are not linearly but exponentially correlated.

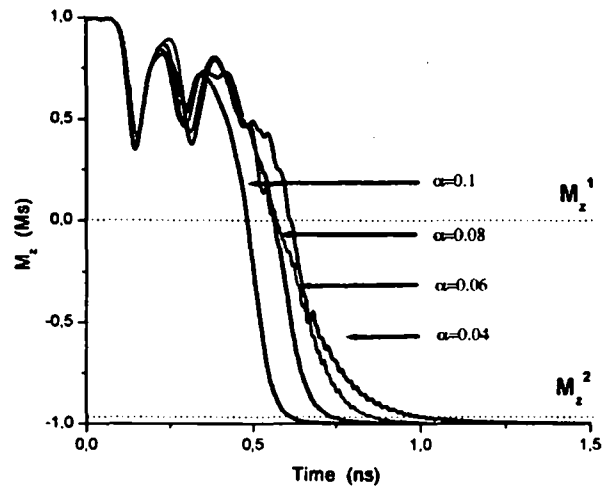


Figure 8.7: Magnetization reversal as a function of Damping constant α versus time (ns), for $\alpha = 0.1, 0.08, 0.06, 0.04$.

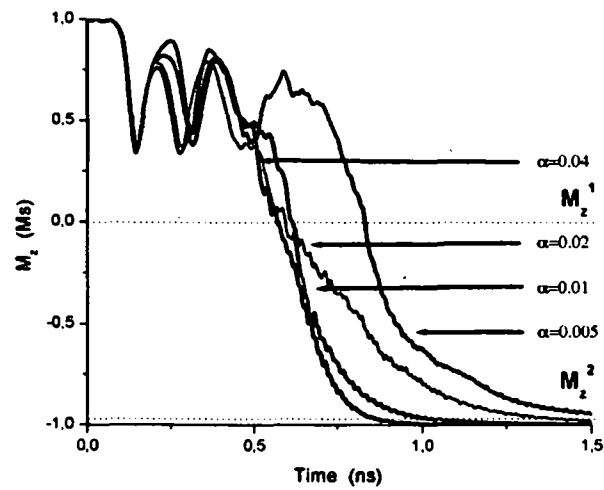


Figure 8.8: Magnetization reversal as a function of Damping constant α versus time (ns), for $\alpha = 0.04, 0.02, 0.01, 0.005$.

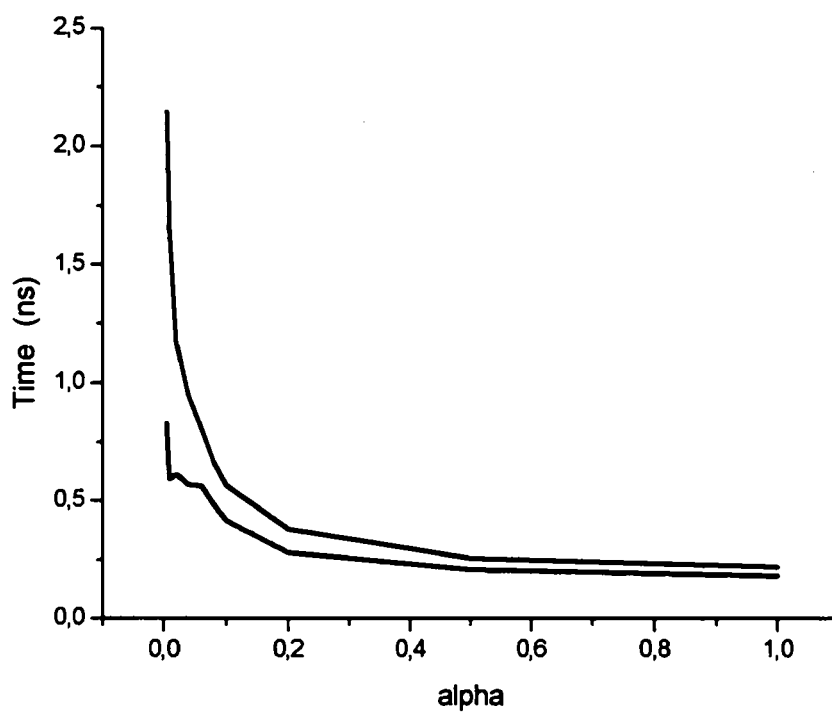


Figure 8.9: Magnetization reversal as a function of Damping constant α versus time (ns). Black plot: values of M_z^1 (time to reach the xy-plane), red plot: values of M_z^2 (time to reach -0.99 ns)

8.3 Precession and Damping Term including Eddy Currents

In the last sections the influence of the Gilbert damping constant on the magnetization reversal was investigated. A high damping leads to a fast magnetization reversal and for low damping it takes the system longer to reach an equilibrium state. Eddy currents are normally not taken into account as a stand alone factor. The underlying assumptions on this fact are either quasi-static approximation, small material conductivity, or that the net contribution of eddy currents is already included in the value of the damping parameter in the Landau-Lifschitz-Gilbert (LLG) equation.

Several attempts were made to include the eddy current effects as a separate contribution to the magnetization process. L. Torres et al. presented a standard 3-dimensional finite difference model, where they solved the LLG equation in conjunction with quasi-static Maxwell equations by introducing the eddy currents with the electric field \mathbf{E} approach [54].

In the model presented in this thesis, eddy current effects are introduced as a eddy current field \mathbf{H}_{eddy} which is directly derived out of the magnetization rate of change. Taking a closer look at the eddy current diffusion equation

$$\sigma\mu_0\frac{\partial\mathbf{M}}{\partial t} = \Delta\mathbf{H}_{\text{eddy}} - \sigma\mu_0\frac{\partial\mathbf{H}_{\text{eddy}}}{\partial t} \quad (8.3.1)$$

the change of the magnetization with time can be deduced as the source term of the eddy current field. Meaning that the eddy current field can be approximated as

$$\mathbf{H}_{\text{eddy}} \simeq \frac{\partial\mathbf{M}}{\partial t} \quad (8.3.2)$$

being proportional to the magnetization rate of change. The advantage of this approach is that the direct influence of the eddy current effects on the precession and on the damping can be studied. The eddy current field is directly introduced as an

additional contribution to the precession

$$\frac{|\gamma_0|}{1 + \alpha^2} \mathbf{M} \times \mathbf{H}_{\text{eddy}} \quad (8.3.3)$$

and to the damping term

$$\frac{|\gamma_0|\alpha}{1 + \alpha^2} \mathbf{M} \times (\mathbf{M} \times \mathbf{H}_{\text{eddy}}). \quad (8.3.4)$$

In Figure 8.10 the eddy field \mathbf{H}_{eddy} and its two torque contributions on the magnetization path are visualized. For small damping reversal is governed by gyromagnetic precession. The precessional motion causes a high $\frac{\partial \mathbf{M}}{\partial t}$ which in turn gives rise to an eddy current field. The $\frac{\partial \mathbf{M}}{\partial t}$ vector is in a plane perpendicular to the applied field. The first term 8.3.3 produces a torque in the precession polar plane with a phase shift due to the direction of the magnetization motion. The phase shift leads to a slowing down of the precession movement which is visualized by plotting either the \mathbf{M}_x or the \mathbf{M}_y component over time, once with and once without eddy current contributions, see Fig. 8.12.

The second term, which is always normal to the precession contribution of the eddy current field, produces a torque in the direction of the applied field acting in the negative azimuthal direction. This term helps to trigger the precessional switching of the magnetization. But once the intermediate state of magnetization reversal is reached the eddy current field leads to a slowing down of the magnetization reversal process, shown in Fig. 8.11. This is due to the torque which is produced by the eddy current damping contribution, which results in a magnetization vector pointing away from the normal magnetization reversal path, shown in Figure 8.10.

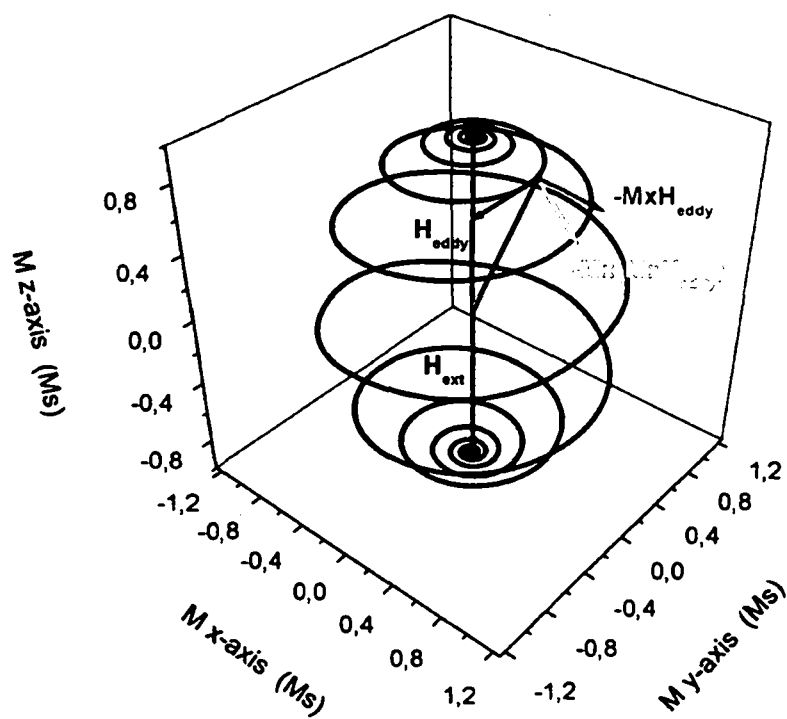


Figure 8.10: Trajectory of the Magnetization Vector over time with eddy current contributions.

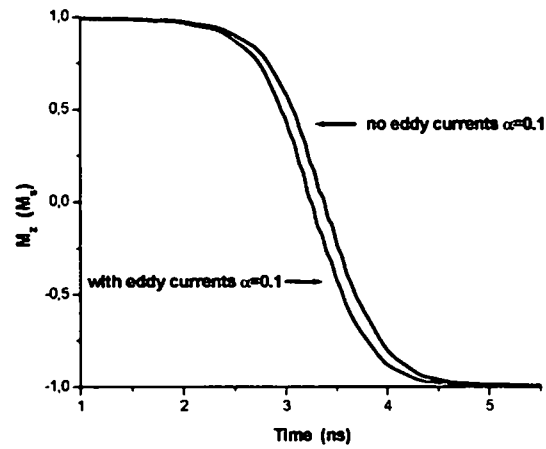


Figure 8.11: Time evolution of M_z for a Permalloy nanocube of 27 nm edge length, a conductivity of $\sigma = 1.10^9 (\Omega\text{m})^{-1}$ and $\alpha = 0.1$ under the influence of an applied field of 200mT.

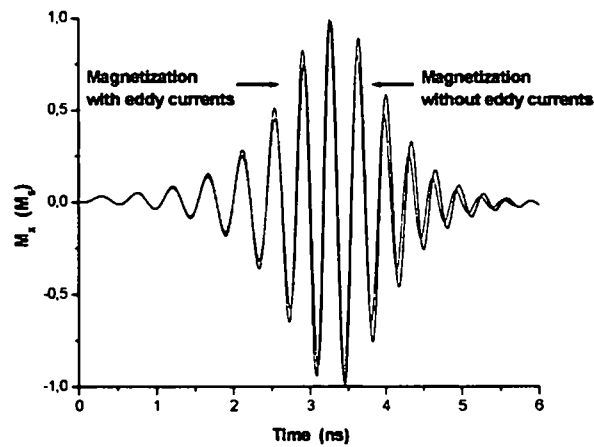


Figure 8.12: Time evolution of M_x for a Permalloy nanocube of 27 nm edge length, a conductivity of $\sigma = 1.10^9 (\Omega\text{m})^{-1}$ and $\alpha = 0.1$ under the influence of an applied field of 200mT.

8.4 Demagnetization Field and Eddy Currents

In our derivation of the eddy current diffusion equation we have made several approximations by omitting the change of the applied field \mathbf{H}_a with time and also the change of the demagnetization field \mathbf{H}_d with time.

The first approximation, the omission of the applied field in our derivation, is justified when the rise time of the applied field is shorter than the precession period. As shown in the previous chapter eddy current effects in small particles are mainly due to gyromagnetic precession. For slow varying external field the field can be approximated as constant during one precession period and therefore the $\frac{\partial \mathbf{H}_a}{\partial t}$ can be neglected in the eddy current diffusion equation.

The omission of the demagnetization field \mathbf{H}_d is somewhat more delicate. The demagnetization field of a cubic sample can be approximated by a demagnetization field of a sphere, as shown by Amikan Aharoni [56]. This means that a value of $\sim \frac{1}{3}M_s$ is expected.

Simulations were performed with a 27 nm edge length nanocube and a saturation magnetization of 1 T. The average demagnetization field was found to be $\sim \frac{1}{3}$ in units of the saturation magnetization. To investigate the influence of the demagnetization field \mathbf{H}_d on the magnetization reversal process including eddy currents, it was substituted in the eddy current diffusion equation

$$\sigma\mu_0 \left(\frac{\partial \mathbf{M}}{\partial t} + \frac{\partial \mathbf{H}_d}{\partial t} \right) = \Delta \mathbf{H}_{\text{eddy}} - \sigma\mu_0 \frac{\partial \mathbf{H}_{\text{eddy}}}{\partial t}. \quad (8.4.1)$$

Simulation were performed with the old diffusion equation and the modified diffusion equation. The calculations show that the change of the demagnetization field with time does not change the magnetization reversal process concerning the eddy current effects, as shown in Fig. 8.13. The demagnetizing field \mathbf{H}_d is proportional to $-M$. Thus the inclusion of \mathbf{H}_d in 8.4.1 is similar to a small change in the conductivity, which turns out to be negligible.

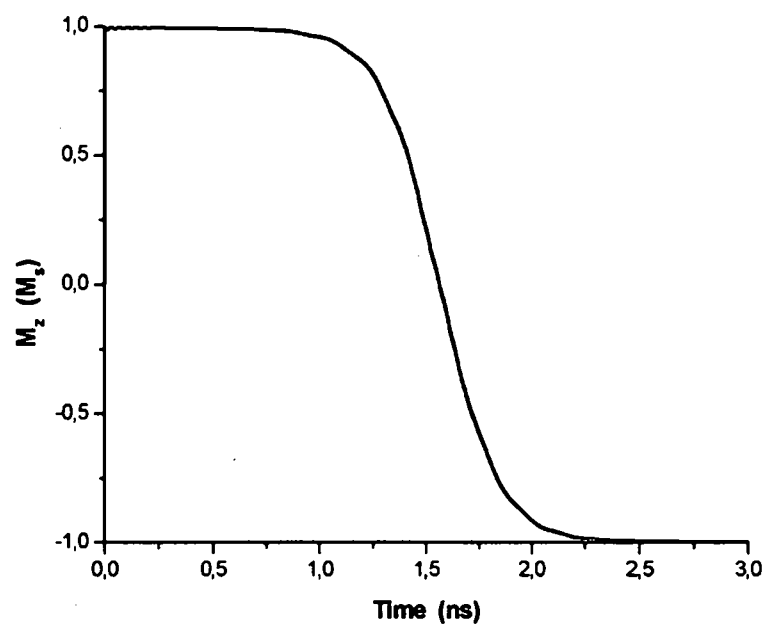


Figure 8.13: Time evolution of M_z for a Permalloy nanocube of 27 nm edge length, a conductivity of $\sigma = 1.10^9 (\Omega\text{m})^{-1}$ and $\alpha = 0.1$ under the influence of an applied field of 200mT: black line, diffusion equation without $\frac{\partial H_d}{\partial t}$, red line, diffusion equation with $\frac{\partial H_d}{\partial t}$.

8.5 Conclusions

In this chapter magnetization reversal simulations of cubic nano scale samples were performed. The impact of different values of the damping parameter on the magnetization reversal process was shown and the magnetization reversal time as a function of the damping value was derived. Small damping gives rise to gyromagnetic precession and therefore a large change of magnetization with time. It is shown that eddy current effects in small particles are a consequence of gyromagnetic precession.

The inclusion of eddy current effects in our calculations show that eddy currents lead to a faster switching of the system at the beginning of the magnetization reversal process. But in the intermediate state of magnetization reversal it leads to a slowing down which takes the system longer to reach the equilibrium state.

The magnitude of the contributions of eddy currents on the damping parameter are not specified easily and will be discussed in more detail in the following chapters.

Chapter 9

Eddy Currents in Sub-Micron Permalloy Structures

In the last chapters it was shown that the dynamic process of magnetization reversal is governed by the Landau–Lifshitz–Gilbert equation which was simulated with a 3-dimensional micromagnetic finite element/boundary element model. In this model each computational cell experiences an effective magnetic field deriving from the total free energy of the system. Gibbs free energy consists of four contributions: exchange, demagnetization, anisotropy and Zeemann. In addition to the mentioned contributions eddy current effects have been included, as the materials used have an appreciable conductivity. From Faradays law, time variations of magnetic induction give rise to an electric field and a current respectively. By means of Ohms and Amperes law, this current induces a new contribution to the total magnetic field, which is called eddy current field \mathbf{H}_{eddy} . This eddy current field is incorporated into the total effective field and the change of the magnetization reversal process is investigated. E. Martinez et al. have developed a micromagnetic model where they calculated the eddy current field by means of the electric field with Bio–Savarts Law. They investigated the influence of eddy currents on reversal processes in nanocubes depending

on size.

In this chapter we use our model to analyze the relevancy of eddy current contributions to the magnetization switching of Permalloy nanocubes. Especially the impact of eddy currents and its governing diffusion equation on the magnetization behavior of materials with different conductivity and size is investigated.

9.1 Diffusion Equation and Material Parameters

The eddy current diffusion equation shows that the eddy current field is directly derived out of the magnetization rate of change, which itself is calculated out of the Landau–Lifshitz–Gilbert equation of motion. To analyze the dependency of the field expression on the material parameters, which are essential in the design of magnetic nanostructures, it is necessary to derive a dimensionless expression of the conditional equations that describe the magnetization process.

By substituting the time t with τ

$$\frac{1}{M_s \gamma_0} \frac{1}{t} = \frac{1}{\tau} \quad (9.1.1)$$

and the eddy current field \mathbf{H}_{eddy} with the normalized field \mathbf{h}_{eddy}

$$\mathbf{h}_{\text{eddy}} = \frac{\mathbf{H}_{\text{eddy}}}{M_s} \quad (9.1.2)$$

and further substituting $d\mathbf{x} = \mathbf{x}$ a dimensionless for the inhomogeneous differential equation of the eddy current field is derived

$$\Delta \mathbf{h}_{\text{eddy}} = \sigma \cdot M_s \cdot \gamma_0 \cdot d^2 \left(\frac{\partial \mathbf{h}_{\text{eddy}}}{\partial \tau} + \frac{\partial \mathbf{m}}{\partial \tau} \right) \quad (9.1.3)$$

where σ is the conductivity, M_s the saturation magnetization, γ_0 the electron gyromagnetic ratio, d the dimension of the sample and $\mathbf{m} = \mathbf{M}/M_s$.

The dimensionless expression of the diffusion equation shows that it is linearly dependant on the conductivity and quadratically dependant on the dimension of the sample.

9.2 Eddy Currents and Material Parameters

The dimensionless expression of the eddy current diffusion equation shows that the eddy current field is dependent on the size of the sample and on the conductivity of the material used. To illustrate the effect of eddy currents, permalloy nanocubes with different edge lengths and different conductivities were simulated. The cubes were discretized with a specific number of tetrahedrons to keep the same elemental size for each sample of 3.4 nm. An external field $\mathbf{B} = -200 \mathbf{u}_z \text{mT}$ was applied to the nanocubes, which were initially magnetized in +z-direction. The applied field increases from zero linearly to its final value at 0.1 ns and remains constant thereafter. First, simulations were performed with a nanocube of 27 nm edge length with two different conductivity values, $\sigma = 1.10^7 (\Omega\text{m})^{-1}$ and $\sigma = 1.10^9 (\Omega\text{m})^{-1}$, shown in Fig. 9.1.

The simulations show that the switching starts at the boundary and begins to propagate into the sample. During this process the eddy currents induce an eddy current field that triggers the precessional switching of the magnetization. Furthermore it can be seen from the simulations performed that the magnetization process starts earlier for high conductivity materials and also leads to a faster magnetization reversal as compared with the simulation results obtained in chapter 8. This can be interpreted as an effectively higher damping caused by eddy currents. Taking a closer look at the precession movement by plotting the x-direction of the magnetization \mathbf{M} over time it can be deduced that a high conductivity leads to a slowing down of the precession movement once the intermediate state of magnetization reversal is reached, see Fig. 9.2.

The next simulations were performed with 20 and 27 nm edge length nanocubes to investigate the impact of the sample size on the eddy current contribution to the

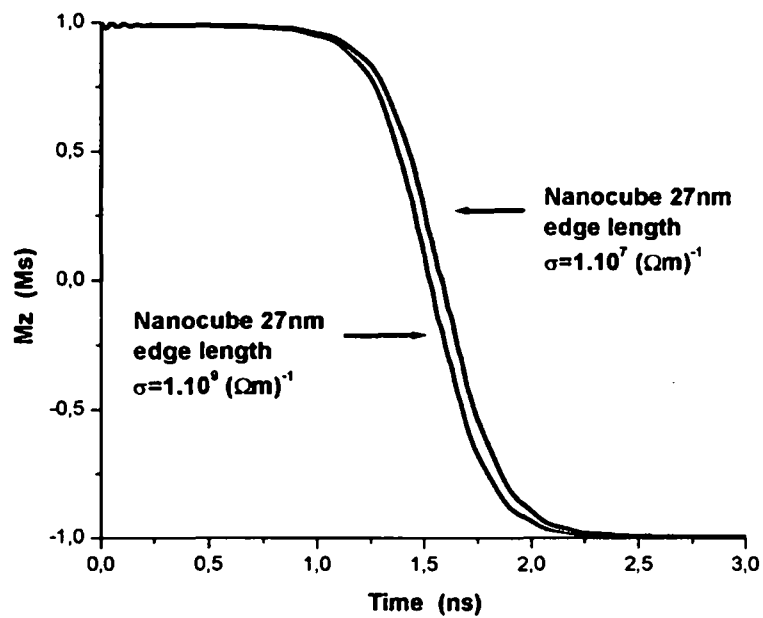


Figure 9.1: Magnetization \mathbf{M} in z -direction as a function of time under an applied field of $\mathbf{B} = -200 \mathbf{u}_z \text{mT}$ and $\alpha = 0.1$. Black line with eddy currents and $\sigma = 1.10^7 (\Omega\text{m})^{-1}$, red line with eddy currents and $\sigma = 1.10^9 (\Omega\text{m})^{-1}$.

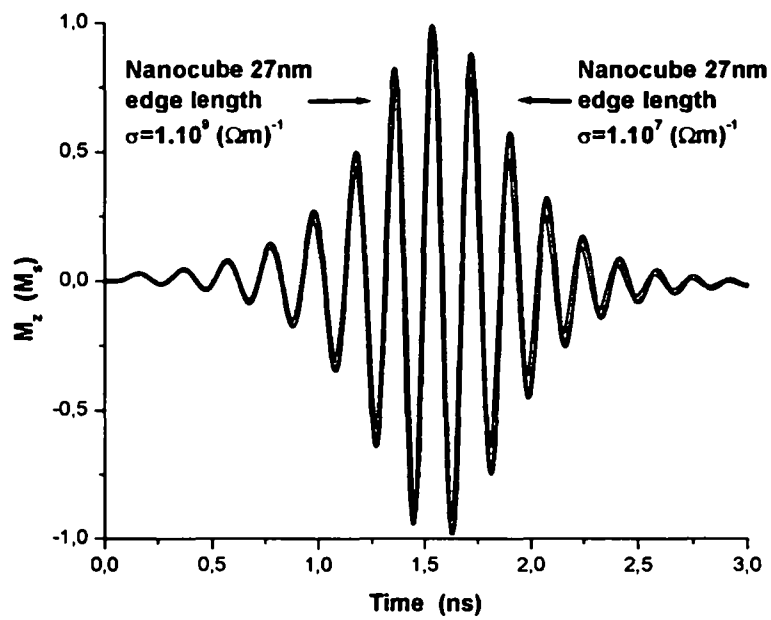


Figure 9.2: Magnetization M in x-direction as a function of time under an applied field of $\mathbf{B} = -200 \mathbf{u}_z \text{mT}$ and $\alpha = 0.1$. Black line with eddy currents and $\sigma = 1.10^7 (\Omega\text{m})^{-1}$, red line with eddy currents and $\sigma = 1.10^9 (\Omega\text{m})^{-1}$.

magnetization switching. In the diffusion equation the size imposes a quadratic dependency on the eddy current behavior and should result in a bigger effect compared to the conductivity as its effect is of linear nature. The results obtained by the simulations show, as expected, a bigger impact of the size of the sample on the relevance of the eddy current contribution to the magnetization reversal process, see Fig. 9.3. Meaning that, the bigger the sample the bigger the eddy current effect. Taking a closer look at the precession movement, see Fig. 9.4 shows that an increase of the sample size leads to a faster precession in the beginning but slows down once the intermediate state of magnetization reversal is reached. The faster precession is seen as an increase in the amplitude of the $M_x(t)$ plot in Fig. 9.4, whereas the slowing down leads to a decrease of the $M_x(t)$ amplitude.

9.3 The Eddy Current Diffusion Parameter

In the last section the influence of the sample size and its conductivity on the magnitude of the eddy current contribution to the magnetization reversal process has been investigated. The two material parameters were separately analyzed regarding their impact on the eddy current effect. But by plotting the diffusion parameter

$$\sigma \cdot M_s \cdot \gamma_0 \cdot d^2 \quad (9.3.1)$$

of the diffusion equation

$$\Delta \mathbf{h}_{\text{eddy}} = \sigma \cdot M_s \cdot \gamma_0 \cdot d^2 \left(\frac{\partial \mathbf{h}_{\text{eddy}}}{\partial \tau} + \frac{\partial \mathbf{m}}{\partial \tau} \right) \quad (9.3.2)$$

for a given magnetization rate of change, a connection between the size, the conductivity and the applied field can be derived. The parameter is plotted to give the magnetization rate of change as a function of conductivity and size, as shown in

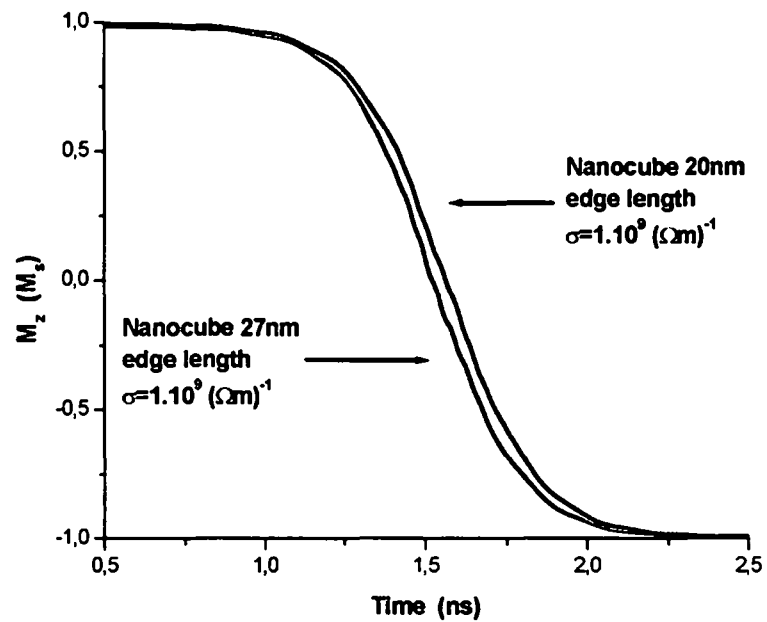


Figure 9.3: Magnetization M in z-direction of a Permalloy nanocube with different sizes as a function of time under an applied field of $\mathbf{B} = -200 \mathbf{u}_z \text{mT}$ and $\alpha = 0.1$. Black line with eddy currents, a conductivity of $\sigma = 1.10^9 (\Omega\text{m})^{-1}$ and an edge length of 20 nm, red line with eddy currents, a conductivity of $\sigma = 1.10^9 (\Omega\text{m})^{-1}$ and an edge length of 27 nm.

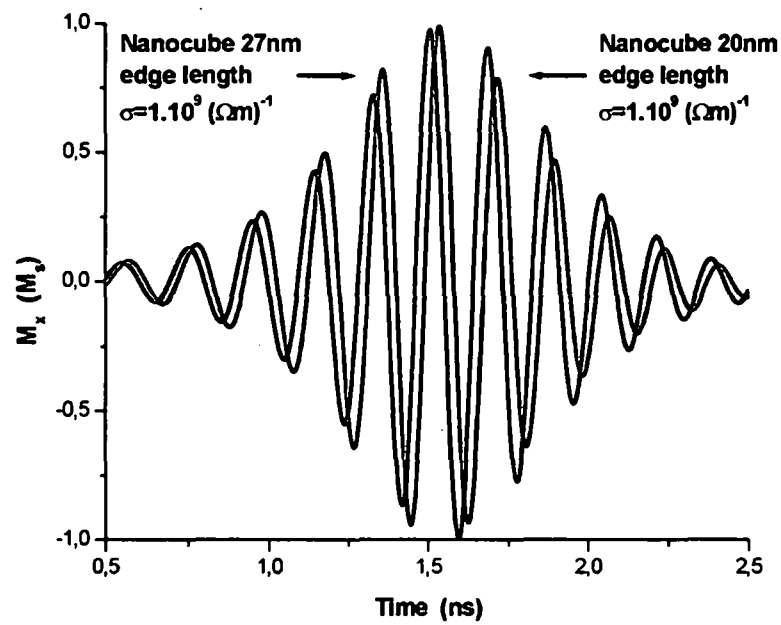


Figure 9.4: Magnetization M in x-direction of a permalloy nanocube with different sizes as a function of time under an applied field of $\mathbf{B} = -200 \mathbf{u}_z \text{mT}$ and $\alpha = 0.1$. Black line with eddy currents, a conductivity of $\sigma = 1.10^9 (\Omega\text{m})^{-1}$ and an edge length of 20 nm, red line with eddy currents, a conductivity of $\sigma = 1.10^9 (\Omega\text{m})^{-1}$ and an edge length of 27 nm.

Fig. 9.5.

Micromagnetic simulations were performed to give the magnetization rate of change for each contour line in Fig. 9.5, as shown in Fig. 9.6. The contour lines give the development of the size–conductivity interaction for a given applied field.

That means that the same magnetization behavior can be achieved by varying the conductivity and the size of the sample with respect to the course of the corresponding phase curve.

For example: Marking a point A on the red curve in Fig. 9.7 and making the corresponding magnetization reversal simulations, doing the same for a second point B, which has different material parameters, the same magnetization behavior is simulated, shown in Fig. 9.8.

9.4 Eddy currents and Critical Size of Single Domain Behavior

In the last section the material parameters which govern the eddy current field contribution were derived and analyzed. The conductivity was shown to increase the contribution and therefore simulating a higher damping constant value. In addition it was shown that the size of the sample has an even greater impact on the magnetization reversal.

Therefore additional simulations were performed with increasing size of the permalloy nanocube. Beginning with an edge length of 20 nm and increasing it thereafter to 27 nm, 33 nm and 40 nm. The results have shown that the eddy current effect increases from 20 to 27 nm, reaches nearly zero with 33 nm, see Fig. 9.9, and increases again at a size of 40 nm, see Fig. 9.10. To understand this effect the spin structure of the sample over time was analyzed.

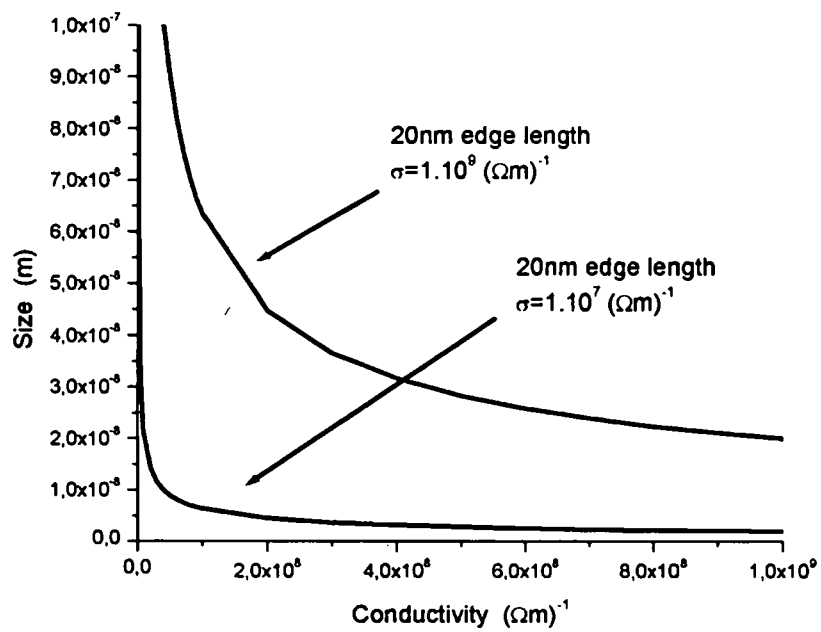


Figure 9.5: Contour lines of the constant prefactor of the eddy current diffusion equation for a fixed magnetization rate. Red line, function for high eddy current contributions (corresponds to red line in Fig. 9.6). Black line, function for low eddy current contributions (corresponds to black line in Fig. 9.6).

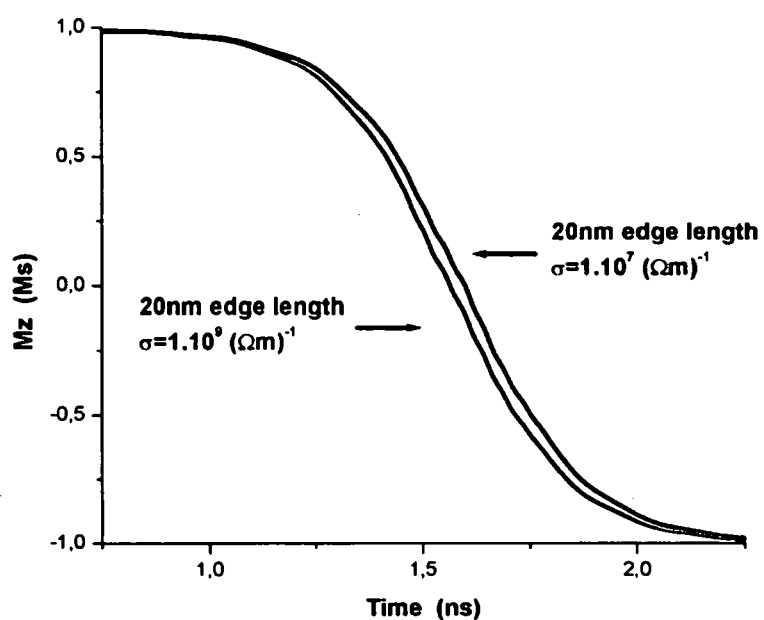


Figure 9.6: Magnetization M in z -direction as a function of time under an applied field of $\mathbf{B} = -200 \mathbf{u}_z \text{mT}$ and $\alpha = 0.1$. Black line with eddy currents and a conductivity of $\sigma = 1.10^9 (\Omega m)^{-1}$, red line with eddy currents and a conductivity of $\sigma = 1.10^9 (\Omega m)^{-1}$.

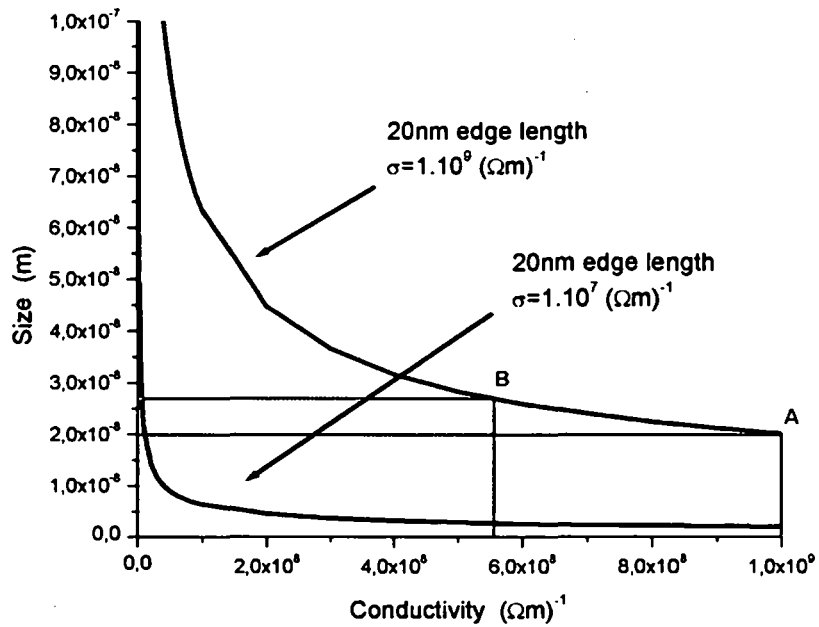


Figure 9.7: Contour lines of the constant prefactor of the eddy current diffusion equation for a fixed magnetization rate. Red line, function for high eddy current contributions (corresponds to red line in Fig. 9.6). Black line, function for low eddy current contributions (corresponds to black line in Fig. 9.6). Point A corresponds to the magnetization behavior of the black line curve in Fig. 9.8 and Point B corresponds to the red line curve in Fig. 9.8

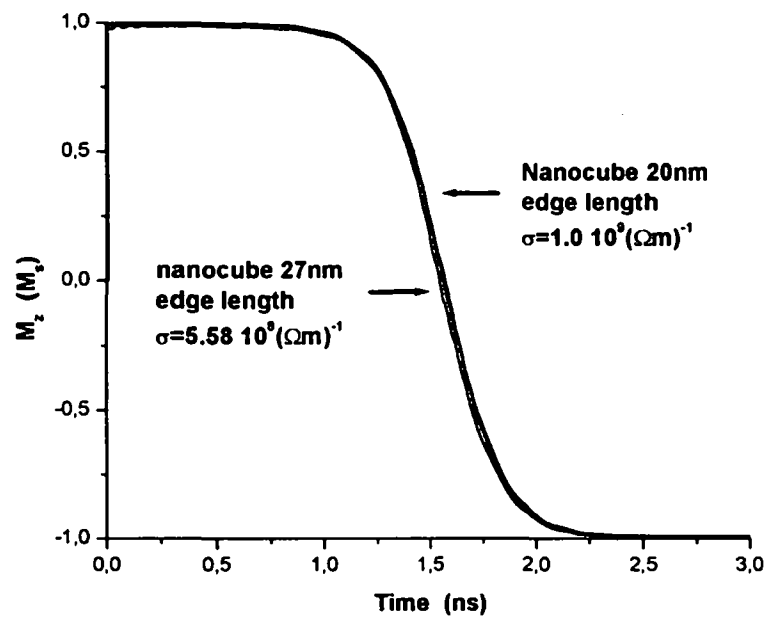


Figure 9.8: Magnetization \mathbf{M} in z-direction of a Permalloy nanocube with different sizes as a function of time under an applied field of $\mathbf{B} = -200 \mathbf{u}_z \text{mT}$ and $\alpha = 0.1$. Black line with eddy currents, a conductivity of $\sigma = 5.58 \cdot 10^8 (\Omega \text{m})^{-1}$ and an edge length of 20 nm, red line with eddy currents, a conductivity of $\sigma = 1.10^9 (\Omega \text{m})^{-1}$ and an edge length of 27 nm.

The initial state is basically magnetized along the easy axis and is called the single domain or flower state. This kind of state is found in the 20 nm and 27 nm samples. Once a field is applied the magnetization reversal process starts and simulations show for these sizes a coherent rotation of all magnetic spins in the system. The magnetization reversal is uniform over time.

In the 33 nm sample, the initial state is a flower state as well, but once the field is applied and although the magnetization reversal starts uniform, it develops into a so called a twisted flower state, a very incoherent spin structure.

In the 40 nm sample, on the other hand, a vortex is formed and wanders through the sample until the system reaches an equilibrium state.

The results of these simulations show that there is a critical size [57] where the flower state of the single domain particle (20 nm and 27 nm) collapses, becomes unstable and develops through curling into a vortex state configuration (40 nm). This transition is accompanied by an intermediate configuration which is largely nonuniform, the twisted flower state configuration (33 nm).

Taking these results and setting them in context to the change of the eddy current contribution, leads to the conclusion that the eddy current effect contribution is connected to the coherence of the magnetic spin structure.

In small particles with a uniform magnetization reversal all the spins are in phase and their single eddy current contributions add up to one big contribution. Once the magnetization reversal becomes nonuniform, as in the twisted flower state, many spins are in different phases and their contributions do not add up anymore leading to a small eddy current contribution. For bigger samples a more uniform magnetization reversal is found, a vortex state configuration, leading to a more significant eddy current contribution.

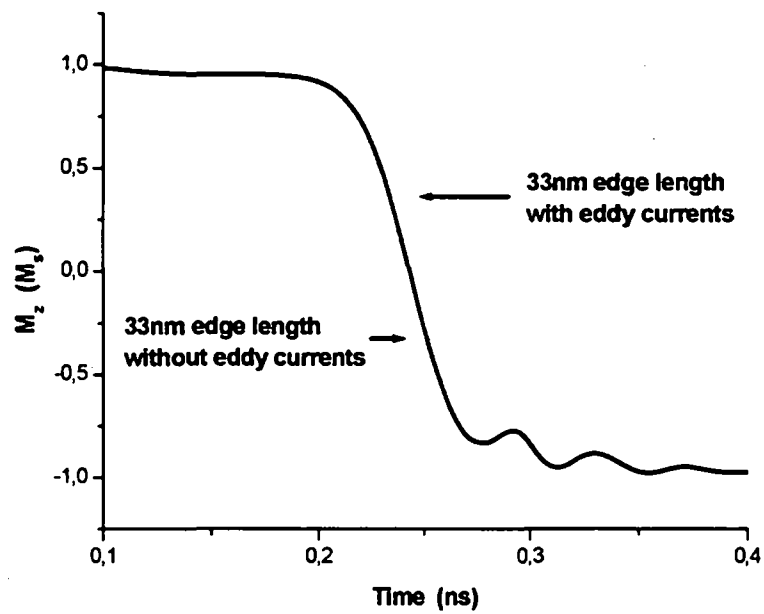


Figure 9.9: Magnetization \mathbf{M} in z-direction of a 33 nm nanocube as a function of time under an applied field of $\mathbf{B} = -200 \mathbf{u}_z \text{mT}$ and $\alpha = 0.1$. Black line without eddy currents and $\alpha = 0.1$, red line with eddy currents, $\alpha = 1$ and a conductivity of $\sigma = 1.10^9 (\Omega\text{m})^{-1}$.

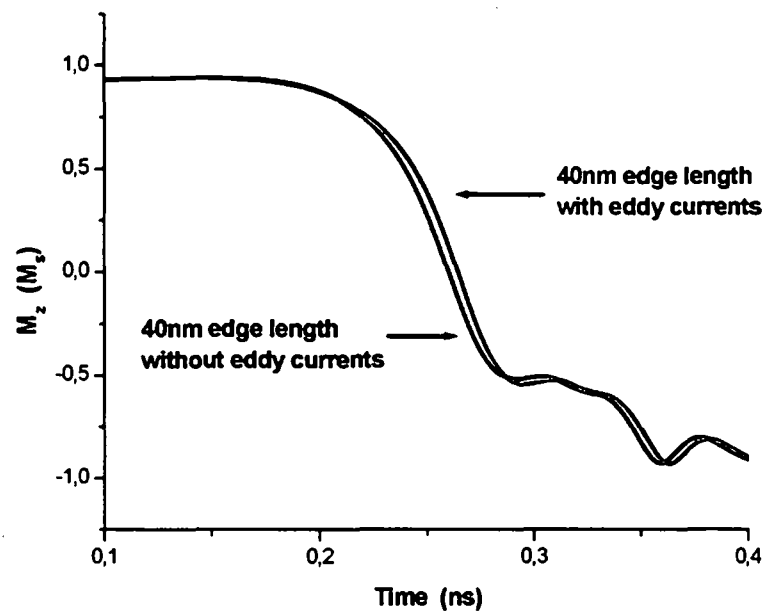


Figure 9.10: Magnetization \mathbf{M} in z -direction of a 40 nm nanocube as a function of time under an applied field of $\mathbf{B} = -200 \mathbf{u}_z \text{mT}$ and $\alpha = 0.1$. Black line without eddy currents and $\alpha = 0.1$, red line with eddy currents, $\alpha = 1$ and a conductivity of $\sigma = 1.10^9 (\Omega\text{m})^{-1}$.

9.5 Conclusions

From the eddy current diffusion equation the governing material parameters, the conductivity and the size, which influence the contributions of the eddy currents to magnetization reversal were derived by normalizing the fields and making the equation dimensionless. The derived diffusion parameter was plotted for a given magnetization behavior. The resulting phase diagram gives the size over the conductivity and shows that the same magnetization behavior can be achieved by varying the conductivity and the size in respect to the contour lines for a given magnetization rate of change. Furthermore it is shown that the size of the sample has a bigger impact on the eddy current contribution compared to the conductivity. Size simulations have further shown that the critical size for a single domain behavior, defined as the maximum size at which magnetization reversal proceeds by rotation in unison, for a cubic sample is lower than 33 nm edge length.

Three kinds of mechanisms of magnetization reversal were found to define the reversal process: spin rotation in unison, non-uniform rotation, and vortex motion.

The size investigations and their impact on the eddy current contributions have shown that the magnitude of the eddy current effect depends on the coherence of the spin structure as follows:

In small particles with a uniform magnetization reversal all the spins rotate in unison and their single eddy current contributions add up to one big contribution. But once the magnetization reversal becomes nonuniform, as it is the case of the twisted flower state, the spins rotation is not in unison and their contributions do not add up anymore leading to a small eddy current contribution. For bigger samples a more uniform magnetization reversal is found, the vortex configuration, leading to a more significant eddy current contribution.

Chapter 10

Influence of Eddy currents on the Effective Damping Parameter

The influence of eddy currents on magnetization dynamics may be incorporated into standard micromagnetic by the use of an effective damping parameter as originally proposed by Chikazumi [58]. However, his theory only applies for large particle where magnetization reversal is dominated by domain wall motion.

Several models were presented in the past to describe magnetization reversal processes for small particles and the transition lengths from multi- to single-domain particles, like by Rave, Fabian and Hubert [59] and Schabes and Bertram [60], however those methods did not include eddy currents. Mayergoyz et al.[61] presented a self-consistent numerical solution of the magnetic diffusion equation and the Landau-Lifshitz equation for linear and circularly polarized applied magnetic fields and showed the effect of eddy currents for different conducting ferromagnetic films. L. Torres et al. [62] developed a micromagnetic model that included eddy currents and investigated the magnetization behavior for high conductivity materials.

In this chapter we use the 3-dimensional micromagnetic model that includes eddy current effects to derive a method to calculate the effective damping parameter as

a function of particle size and electric conductivity for single domain particles. We use this model to simulate magnetization reversal processes in sub-micron permalloy structures and investigate the total energy of the system under different applied fields and different material parameters. From the change of energy with time an effective damping parameter is calculated [63]. By comparing the calculated effective parameter with the imposed damping constant value, the net eddy current contribution to the dynamic magnetization processes is determined.

10.1 Model

In order to derive how the damping parameter is related to the change of energy with time we first recall the LLG equation and the eddy current diffusion equation in dimensionless form.

To describe the dynamic magnetization process in single domain particles, we start from the Landau–Lifshitz–Gilbert equation of motion, whereby all vector quantities \mathbf{H}_{eff} and \mathbf{H}_{eddy} are normalized by the saturation magnetization M_s , as shown for the effective field

$$\mathbf{h}_{\text{eff}} = \frac{\mathbf{H}_{\text{eff}}}{M_s}, \quad \mathbf{m} = \frac{\mathbf{M}}{M_s} \quad (10.1.1)$$

with μ_0 being the permeability of free space. Furthermore a reduced time τ is introduced

$$\tau = M_s \gamma_0 t \quad (10.1.2)$$

where $\gamma_0 > 0$ denotes the gyromagnetic ratio. With the conventions defined in equation 10.1.1 and 10.1.2 a dimensionless expression for the Landau–Lifshitz–Gilbert equation is derived

$$(1 + \alpha^2) \frac{\partial \mathbf{m}}{\partial \tau} = -(\mathbf{m} \times \mathbf{h}_{\text{eff}}) - \alpha \mathbf{m} \times (\mathbf{m} \times \mathbf{h}_{\text{eff}}) \quad (10.1.3)$$

where α is a dimensionless empiric damping parameter, called Gilbert damping constant. The effective field in 10.1.3, which is composed of the anisotropy contribution \mathbf{h}_{ani} , the exchange field \mathbf{h}_{exch} , the applied field \mathbf{h}_{a} and the magnetostatic field \mathbf{h}_{M} , is derived from a variational analysis, as the coefficient of the first variation of the Gibbs free energy functional [64].

Eddy current effects are introduced by an eddy current field \mathbf{h}_{eddy} , which is a part of the effective field \mathbf{h}_{eff} , and is calculated by solving the eddy current diffusion equation. Applying the vector normalization and the reduced time on the diffusion equation yields

$$\Delta \mathbf{h}_{\text{eddy}} = \sigma \cdot M_s \cdot \gamma_0 \cdot d^2 \left(\frac{\partial \mathbf{h}_{\text{eddy}}}{\partial \tau} + \frac{\partial \mathbf{m}}{\partial \tau} \right) \quad (10.1.4)$$

where σ is the conductivity and d is the dimension of the particle. The dimensionless expression of the conditional equations shows that the diffusion of the field is linearly dependent on the conductivity and quadratically dependant on the size. Equation 10.1.3 and 10.1.4 are a coupled system of LLG and quasi-static Maxwell equations and are solved by a hybrid finite element/boundary element method [65] [66].

10.2 Eddy Currents and the Effective Damping Parameter

To determine the contribution of eddy currents on the total energy dissipation rate of a dynamic micromagnetic system a self-consistent criteria proposed by Albuquerque [63] is used.

The energy dissipation rate depends only on intrinsic material parameters and on the actual magnetization motion. By disregarding the damping term in 10.1.3 a constant applied field would result only in a precessional motion of the magnetization and therefore leave the energy of the system constant. Consequently no energy is

dissipated.

The introduction of damping results in an irreversible switching of the system, thus the change of energy over time indicates the magnitude of the dissipation and the damping parameter, respectively.

The general expression of the rate of change of the systems free energy functional is given by [64]

$$\frac{\partial E}{\partial \tau} = -M_s^2 \int \mathbf{h}_{\text{eff}} \cdot \frac{\partial \mathbf{m}}{\partial \tau} dV. \quad (10.2.1)$$

Equation 10.2.1 shows that the change of energy is proportional to the change of magnetization integrated over the whole volume, meaning that by rearranging the LLG equation and substituting it into 10.2.1 an expression for the damping parameter α can be derived.

Starting from the Gilbert form of the Landau–Lifshitz–Gilbert equation in the dimensionless form

$$\frac{\partial \mathbf{m}}{\partial \tau} = -\mathbf{m} \times \mathbf{h}_{\text{eff}} + \alpha \left(\mathbf{m} \times \frac{\partial \mathbf{m}}{\partial \tau} \right). \quad (10.2.2)$$

Multiplying equation 10.2.2 respectively with \mathbf{h}_{eff} and $\frac{\partial \mathbf{m}}{\partial \tau}$ yields

$$\mathbf{h}_{\text{eff}} \cdot \frac{\partial \mathbf{m}}{\partial \tau} = -\mathbf{h}_{\text{eff}} \cdot (\mathbf{m} \times \mathbf{h}_{\text{eff}}) + \alpha \mathbf{h}_{\text{eff}} \cdot \left(\mathbf{m} \times \frac{\partial \mathbf{m}}{\partial \tau} \right) \quad (10.2.3)$$

and

$$\frac{\partial \mathbf{m}}{\partial \tau} \cdot \frac{\partial \mathbf{m}}{\partial \tau} = -\frac{\partial \mathbf{m}}{\partial \tau} \cdot (\mathbf{m} \times \mathbf{h}_{\text{eff}}) + \alpha \frac{\partial \mathbf{m}}{\partial \tau} \cdot \left(\mathbf{m} \times \frac{\partial \mathbf{m}}{\partial \tau} \right). \quad (10.2.4)$$

The first term on the right hand side in 10.2.3 and the second term on the right hand side in 10.2.4 vanish as the cross product of two identical vectors are zero. Furthermore the following vector identity

$$\mathbf{A} \cdot (\mathbf{B} \times \mathbf{C}) = -\mathbf{C} \cdot (\mathbf{B} \times \mathbf{A}) \quad (10.2.5)$$

is used on the second term of equation 10.2.3, which recasts the two equations to

$$\mathbf{h}_{\text{eff}} \cdot \frac{\partial \mathbf{m}}{\partial \tau} = -\alpha \frac{\partial \mathbf{m}}{\partial \tau} \cdot (\mathbf{m} \times \mathbf{h}_{\text{eff}}) \quad (10.2.6)$$

and

$$\left(\frac{\partial \mathbf{m}}{\partial \tau}\right)^2 = -\frac{\partial \mathbf{m}}{\partial \tau} \cdot (\mathbf{m} \times \mathbf{h}_{\text{eff}}). \quad (10.2.7)$$

Substituting equation 10.2.7 into equation 10.2.6 yields

$$\mathbf{h}_{\text{eff}} \cdot \frac{\partial \mathbf{m}}{\partial \tau} = \alpha \left(\frac{\partial \mathbf{m}}{\partial \tau}\right)^2 \quad (10.2.8)$$

which is the integral kernel on the right hand side of 10.2.1. By substituting 10.2.8 into 10.2.1

$$\frac{\partial \mathbf{E}}{\partial \tau} = -\alpha M_s^2 \int \left(\frac{\partial \mathbf{m}}{\partial \tau}\right)^2 dV. \quad (10.2.9)$$

and rearranging the new expression yields

$$\alpha = -\frac{1}{M_s^2} \cdot \left[\frac{\partial \mathbf{E}}{\partial \tau} / \int \left(\frac{\partial \mathbf{m}}{\partial \tau}\right)^2 dV \right]. \quad (10.2.10)$$

Since the damping parameter from 10.2.10 is calculated from the simulation results it is called the dynamic damping parameter α_e . For single domain particles, we assume that the magnetic system is rotating in unison as a single magnetic vector. In this case equation 10.2.10 can be approximated with

$$\alpha_e = -\frac{1}{M_s^2} \cdot \left[\frac{\partial \langle \mathbf{E} \rangle}{\partial \tau} / \left(\frac{\partial \langle \mathbf{m} \rangle}{\partial \tau} \right)^2 \right] \quad (10.2.11)$$

its equivalent for a macrospin. Once the magnetization rate of change with and without eddy current effects has been obtained the damping parameter α_e , obtained during the dynamical calculations, can be compared with the imposed damping value α , see Fig. 10.1. Hence the net eddy contributions are determined.

10.3 Permalloy Single Particle Simulations

Simulations are made with cubic permalloy single domain particles of 20nm / 27nm / 33nm / 40nm edge length and a resistivity of $1 \cdot 10^{-8} / 1 \cdot 10^{-9} \Omega \text{m}$. An external applied field of $\mathbf{B}_{\text{ext}} = \mu_0 \mathbf{H}_{\text{ext}} = -100/200/800 \mathbf{u}_z \text{mT}$ is applied to the nanocube, which is

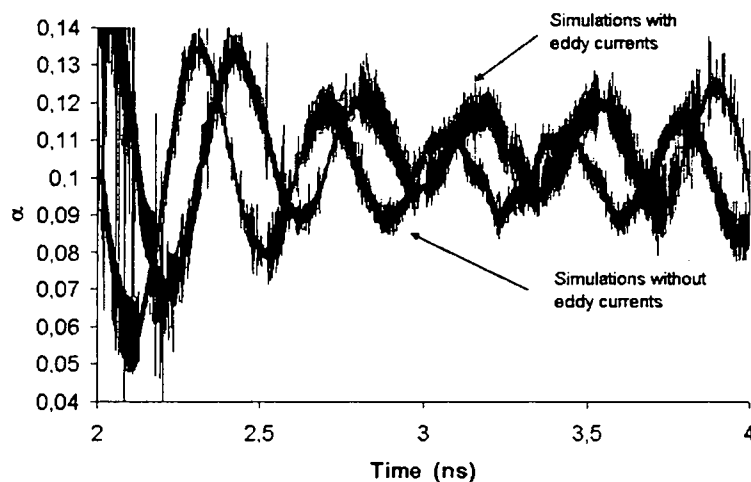


Figure 10.1: The dynamic damping parameter α_e over time for a 27nm edge length nano particle with and without eddy current contributions at an applied field of 100mT.

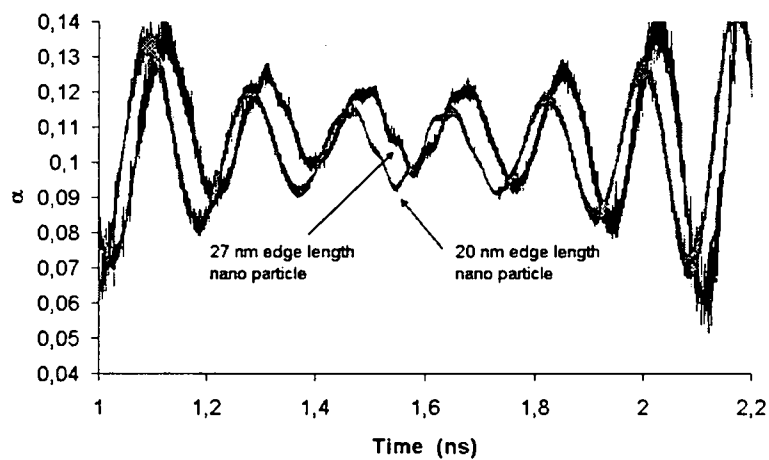


Figure 10.2: The dynamic parameter α_e over time for a 20nm and a 27nm edge length nano particle at an applied field of 200mT.

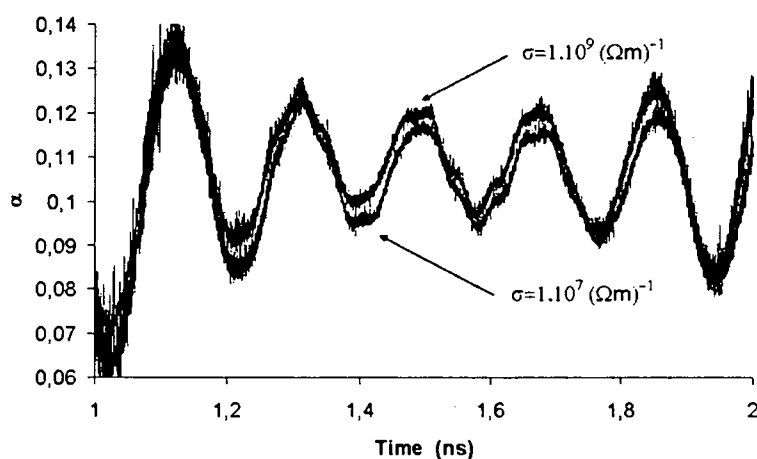


Figure 10.3: The dynamic parameter for a 27nm edge length particle with a low conductivity of $\sigma = 1.10^7(\Omega\text{m})^{-1}$ and a high conductivity of $\sigma = 1.10^9(\Omega\text{m})^{-1}$ at an applied field of 200mT.

initially magnetized in +z-direction. The external field increases from zero linearly to its final value at 0.1ns and remains constant thereafter.

consistency check

First we performed simulations with $\sigma = 0$. As there are no eddy current effects the dynamic calculated α_e is equal to the imposed damping constant α , shown in Table 10.1. α_e is obtained by averaging over the simulated values in Fig. 10.1 to 10.3.

influence of conductivity

Simulations of 27nm particles with a resistivity of $1.10^{-7}\Omega\text{m}$ show an increase of the damping constant by 6 percent in an applied field of 100mT. A lower resistivity of $1.10^{-9}\Omega\text{m}$ leads to an increase 10 percent, shown in Fig. 10.3.

applied field

By increasing the field to 200mT the contribution of the eddy currents decreases to a value of 5 percent and vanishes for fields higher than 800mT. If the external field is high the magnetic field created by eddy currents becomes negligible. The eddy current field is proportional to the change of the magnetization with time but in addition it is also a function of time according to the eddy current diffusion equation 10.1.4. At the beginning of the reversal process, the eddy current field is zero and it will increase with time at a certain rate which depend on σ , γ_0 and d^2 only and does not depend on H_{ext} . On the other hand the time for magnetization reversal decreases with increasing H_{ext} . For large external fields the particle becomes reversed before a significant eddy current contribution is built up.

size

For smaller particles (edge length of 20nm) the contributions of the eddy currents to effective damping are 4 percent, shown in Fig. 10.2, and show the same behavior as the 27nm particles concerning resistivity and field strength. Increasing the particle size to 33nm, however, the critical transition length from homogeneous to inhomogeneous magnetization reversal is reached. The magnetic field created by the eddy currents becomes non-uniform, resulting in an incoherent spin structure leading to a vanishing eddy current contribution to damping of less than 1 percent. All the simulation results are summarized and shown in Table 10.1.

10.4 Conclusions

A model was introduced to calculate the contribution of the eddy currents to the effective damping of the system. Relating the change of the total energy with time to the change of the magnetization with time an effective damping was calculated.

Table 10.1: Gives the simulation and calculation results for the dynamic damping parameter in dependency of field strength, conductivity and size of the sample.

Time (ns)	Size (nm)	H_{ext} (mT)	σ (Ωm)	α	α_e	α_e/α
1.0-2.2	20	200	0	0.1	0.101	1
1.0-2.2	20	200	1.10^{-9}	0.1	0.104	2.97
1.0-2.2	27	200	0	0.1	0.103	1
1.0-2.2	27	200	1.10^{-8}	0.1	0.106	2.91
1.0-2.2	27	200	1.10^{-9}	0.1	0.108	4.85
1.5-4.0	27	100	0	0.1	0.1	1
1.5-4.0	27	100	1.10^{-9}	0.1	0.11	10

Any effective damping higher than the imposed Gilbert damping constant has to be attributed to eddy currents. In small particles, eddy currents may increase the effective damping by up to 10 percent. It was shown that the magnitude of the contribution of eddy currents to the energy dissipation of the system depends on material parameters like the conductivity and the size of the particles. The lower the resistivity of a system the higher the eddy current effect. In the regime of uniform rotation, the eddy current distribution to damping increases with particle size.

List of Figures

2.1	Domain of interest is divided into triangular elements (2D).	20
2.2	Hat-function	21
3.1	Precessional motion of magnetization.	28
4.1	Sample with an anisotropic shape with a magnetic field applied in two perpendicular directions: (right) parallel to the short axis; here the free poles are separated by a relatively short distance, leading to a large \mathbf{H}_d , (left) parallel to the long axis; poles separated by a smaller distance, which leads to a small value of \mathbf{H}_d	38
6.1	Infinitely thin test volume $\hat{\Omega}$ on the boundary $\partial\Omega$	55
8.1	Domain of interest discretized with tetrahedral basis-functions.	65
8.2	Delaunay-Triangulation.	66
8.3	Trajectory of the Magnetization Vector over time.	68
8.4	Trajectory of the Magnetization Vector over time, for high damping.	69
8.5	Trajectory of the Magnetization Vector over time, for low damping.	69
8.6	Magnetization reversal as a function of Damping constant α versus time (ns), for $\alpha = 1, 0.5, 0.2, 0.1$	71
8.7	Magnetization reversal as a function of Damping constant α versus time (ns), for $\alpha = 0.1, 0.08, 0.06, 0.04$	72

- 8.8 Magnetization reversal as a function of Damping constant α versus time (ns), for $\alpha = 0.04, 0.02, 0.01, 0.005$ 72
- 8.9 Magnetization reversal as a function of Damping constant α versus time (ns). Black plot: values of M_z^1 (time to reach the xy-plane), red plot: values of M_z^2 (time to reach -0.99 ns). 73
- 8.10 Trajectory of the Magnetization Vector over time with eddy current contributions. 76
- 8.11 Time evolution of M_z for a Permalloy nanocube of 27 nm edge length, a conductivity of $\sigma = 1.10^9 (\Omega\text{m})^{-1}$ and $\alpha = 0.1$ under the influence of an applied field of 200mT. 77
- 8.12 Time evolution of M_x for a Permalloy nanocube of 27 nm edge length, a conductivity of $\sigma = 1.10^9 (\Omega\text{m})^{-1}$ and $\alpha = 0.1$ under the influence of an applied field of 200mT. 77
- 8.13 Time evolution of M_z for a Permalloy nanocube of 27 nm edge length, a conductivity of $\sigma = 1.10^9 (\Omega\text{m})^{-1}$ and $\alpha = 0.1$ under the influence of an applied field of 200mT: black line, diffusion equation without $\frac{\partial \mathbf{H}_d}{\partial t}$, red line, diffusion equation with $\frac{\partial \mathbf{H}_d}{\partial t}$ 79
- 9.1 Magnetization \mathbf{M} in z-direction as a function of time under an applied field of $\mathbf{B} = -200 \mathbf{u}_z \text{mT}$ and $\alpha = 0.1$. Black line with eddy currents and $\sigma = 1.10^7 (\Omega\text{m})^{-1}$, red line with eddy currents and $\sigma = 1.10^9 (\Omega\text{m})^{-1}$ 84
- 9.2 Magnetization \mathbf{M} in x-direction as a function of time under an applied field of $\mathbf{B} = -200 \mathbf{u}_z \text{mT}$ and $\alpha = 0.1$. Black line with eddy currents and $\sigma = 1.10^7 (\Omega\text{m})^{-1}$, red line with eddy currents and $\sigma = 1.10^9 (\Omega\text{m})^{-1}$. 85

- 9.3 Magnetization \mathbf{M} in z-direction of a Permalloy nanocube with different sizes as a function of time under an applied field of $\mathbf{B} = -200 \mathbf{u}_z \text{mT}$ and $\alpha = 0.1$. Black line with eddy currents, a conductivity of $\sigma = 1.10^9(\Omega\text{m})^{-1}$ and an edge length of 20 nm, red line with eddy currents, a conductivity of $\sigma = 1.10^9(\Omega\text{m})^{-1}$ and an edge length of 27 nm. . . . 87
- 9.4 Magnetization \mathbf{M} in x-direction of a permalloy nanocube with different sizes as a function of time under an applied field of $\mathbf{B} = -200 \mathbf{u}_z \text{mT}$ and $\alpha = 0.1$. Black line with eddy currents, a conductivity of $\sigma = 1.10^9(\Omega\text{m})^{-1}$ and an edge length of 20 nm, red line with eddy currents, a conductivity of $\sigma = 1.10^9(\Omega\text{m})^{-1}$ and an edge length of 27 nm. . . . 88
- 9.5 Contour lines of the constant prefactor of the eddy current diffusion equation for a fixed magnetization rate. Red line, function for high eddy current contributions (corresponds to red line in Fig. 9.6). Black line, function for low eddy current contributions (corresponds to black line in Fig. 9.6). 90
- 9.6 Magnetization \mathbf{M} in z-direction as a function of time under an applied field of $\mathbf{B} = -200 \mathbf{u}_z \text{mT}$ and $\alpha = 0.1$. Black line with eddy currents and a conductivity of $\sigma = 1.10^9(\Omega\text{m})^{-1}$, red line with eddy currents and a conductivity of $\sigma = 1.10^9(\Omega\text{m})^{-1}$ 91
- 9.7 Contour lines of the constant prefactor of the eddy current diffusion equation for a fixed magnetization rate. Red line, function for high eddy current contributions (corresponds to red line in Fig. 9.6). Black line, function for low eddy current contributions (corresponds to black line in Fig. 9.6). Point A corresponds to the magnetization behavior of the black line curve in Fig. 9.8 and Point B corresponds to the red line curve in Fig. 9.8. 92

- 9.8 Magnetization \mathbf{M} in z-direction of a Permalloy nanocube with different sizes as a function of time under an applied field of $\mathbf{B} = -200 \mathbf{u}_z \text{mT}$ and $\alpha = 0.1$. Black line with eddy currents, a conductivity of $\sigma = 5.58 \cdot 10^8 (\Omega\text{m})^{-1}$ and an edge length of 20 nm, red line with eddy currents, a conductivity of $\sigma = 1.10^9 (\Omega\text{m})^{-1}$ and an edge length of 27 nm. 93
- 9.9 Magnetization \mathbf{M} in z-direction of a 33 nm nanocube as a function of time under an applied field of $\mathbf{B} = -200 \mathbf{u}_z \text{mT}$ and $\alpha = 0.1$. Black line without eddy currents and $\alpha = 0.1$, red line with eddy currents, $\alpha = 1$ and a conductivity of $\sigma = 1.10^9 (\Omega\text{m})^{-1}$ 95
- 9.10 Magnetization \mathbf{M} in z-direction of a 40 nm nanocube as a function of time under an applied field of $\mathbf{B} = -200 \mathbf{u}_z \text{mT}$ and $\alpha = 0.1$. Black line without eddy currents and $\alpha = 0.1$, red line with eddy currents, $\alpha = 1$ and a conductivity of $\sigma = 1.10^9 (\Omega\text{m})^{-1}$ 96
- 10.1 The dynamic damping parameter α_e over time for a 27nm edge length nano particle with and without eddy current contributions at an applied field of 100mT. 103
- 10.2 The dynamic parameter α_e over time for a 20nm and a 27nm edge length nano particle at an applied field of 200mT. 103
- 10.3 The dynamic parameter for a 27nm edge length particle with a low conductivity of $\sigma = 1.10^7 (\Omega\text{m})^{-1}$ and a high conductivity of $\sigma = 1.10^9 (\Omega\text{m})^{-1}$ at an applied field of 200mT. 104

Bibliography

- [1] P. G. Ciarlet, *The Finite Element Method for Elliptic Problems*. Amsterdam, New York, Oxford: North-Holland, 1978.
- [2] R. Ribo, M. A. de Riera Pasenau, and E. Escolano, GiD home page, 2002. International Center For Numerical Methods in Engineering (CIMNE), URL: <http://gid.cimne.upc.es>.
- [3] C. Cohen-Tannoudji, B. Diu, and F. Laloe, *Quantum Mechanics* (John Wiley and Sons, New York, 1977).
- [4] C. T. Chen, Y. U. Idzerda, H. J. Lin, N. V. Smith, G. Meigs, E. Chaban, G. H. Ho, E. Pellegrin, and F. Sette, Experimental confirmation of the X-ray magnetic circular dichroism sum rules for iron and cobalt, *Phys. Rev. Lett.* 75, 152–155 (1995).
- [5] H. Goldstein, *Classical Mechanics*. Reading, MA: Addison-Wesley, 1950, pp. 21 and 341
- [6] T. L. Gilbert, A Lagrangian formulation of the gyromagnetic equation of the magnetization field, *Phys. Rev.* 100, pp. 1243 (1955), abstract only.
- [7] L. D. Landau and E. Lifshitz, On the theory of the dispersion of magnetic permeability in ferromagnetic bodies, *Phys. Z. Sowjetunion* 8, pp. 153–169 (1935).

- [8] Brown Jr. W F 1963 *Micromagnetics*. Interscience, New York
- [9] Aharoni A. (1996) *Introduction to the Theory of Ferromagnetism*. Oxford University
- [10] Dahlberg, E. D., Zhu, J. G. (1995) *Micromagnetic Microscopy and Modeling*. *Physics Today* 48, pp. 34-40 Press, New York
- [11] Schabes, M. E., Fullerton, E. E., Margulies, D. T. (2001) *Theory of Antiferromagnetically Coupled Magnetic Recording Media*. *J. Appl. Phys.*,
- [12] Johnson, M. Magneto-electronic memories last and last *IEEE Spectrum* 37, pp. 33-40, 2000.
- [13] D. R. Fredkin and T.R. Koehler ,Hybrid Method for Computing Demagnetizin Fields, *IEEE Trans. Magn.* 26, pp. 415-417, March 1990.
- [14] J. D. Jackson, *Classical Electrodynamics*, pp. ??-?? New York: Wiley 1998.
- [15] F. Bloch, Theory of exchange problem and remanence phenomena of ferromagnetic substances, *Z. Physik*, vol. 74, pp. 295-335, 1932.
- [16] L. D. Landau and E. M. Lifshitz, On the theory of the dispersion of magnetic permeability in ferromagnetic bodies, *Phys. Z. Sowjet.*, vol. 8, pp. 153-169, 1935. In L. D. Landau, *Collected Papers*. ed. by D. ter Haar. Gordon and Breach, New York, 1967, p. 101.
- [17] W. Dring, On the inertia of the walls between Weiss domains, *Zeit. Naturforsch.*, vol. 3a, pp. 373-379, 1948.
- [18] C. Kittel, On the theory of ferromagnetic resonance absorption, *Phys. Rev.*, vol. 73, pp. 155-161, 1948.

- [19] L. Nel, Thorie du trainage magntique de diffusion, *J. Phys. Radium*, vol. 13, pp. 249–264, 1952. P. W. Readman (translator), Theory of the diffusion after-effect, in *Selected Works of Louis Nel*. N. Kurti, ed. Gordon and Breach, New York, 1988, pp. 369–384.
- [20] C. Herring and C. Kittel, On the theory of spin waves in ferromagnetic media, *Phys. Rev.*, vol. 81, pp. 869–880, Mar. 1951.
- [21] W. S. Ament and G. T. Rado, Electromagnetic effects of spin wave resonance in ferromagnetic metals, *Phys. Rev.*, vol. 97, pp. 1558–1566, Mar. 1955.
- [22] P. W. Anderson and H. Suhl, Instability in the motion of ferromagnets at high microwave power levels, *Phys. Rev.*, vol. 100, pp. 1788–1789, Dec. 1955.
- [23] A. M. Clogston, H. Suhl, L. R. Walker, and P. W. Anderson, Possible source of line width in ferromagnetic resonance, *Phys. Rev.*, vol. 101, pp. 903–905, Jan. 1956.
- [24] J. L. Snoek, Time effects in magnetisation, *Physica*, vol. 5, pp. 663–688, 1938.
- [25] H. P. J. Wijn and H. van der Heide, A Richter type after-effect in ferrites containing ferrous and ferric ions, *Rev. Mod. Phys.*, vol. 25, pp. 98–99, Jan. 1953.
- [26] G. T. Rado, On the inertia of oscillating ferromagnetic domain walls, *Phys. Rev.*, vol. 83, pp. 821–826, Aug. 1951.
- [27] J. K. Galt, Motion of individual domain walls in a nickel-iron ferrite, *Bell Syst. Tech. J.*, vol. 33, pp. 1023–1054, 1954.
- [28] L. Nel, Le trainage magntique, *J. Phys. Rad.*, vol. 12, pp. 339351, 1951. P. W. Readman (translator), The magnetic after-effect, in *Selected Works of Louis Nel*. N. Kurti, ed. Gordon and Breach, New York, 1988, pp. 356–368.

- [29] C. E. Webb and L. H. Ford, The time-decrease of permeability at low magnetizing forces, *J. Inst. Elect. Eng. (London)*, vol. 75, pp. 787–797, 1954.
- [30] T. Holstein and H. Primakoff, Field dependence of the intrinsic domain magnetization of a ferromagnet, *Phys. Rev.*, vol. 58, pp. 1098–1113, 1940.
- [31] C. Kittel, Physical theory of ferromagnetic domains, *Rev. Mod. Phys.*, vol. 21, pp. 541–583, 1949.
- [32] P.W. Anderson, The concept of spin-lattice relaxation in ferromagnetic materials, *Phys. Rev.*, vol. 88, p. 1214, Dec. 1952.
- [33] R. Becker, The effective mass of a Bloch wall, *Z. Physik*, vol. 133, pp. 134–139, 1952.
- [34] C. Zener, *Elasticity and Anelasticity of Metals*. Chicago, IL: Univ. of Chicago Press, 1948.
- [35] C. Kittel and E. Abrahams, Relaxation process in ferromagnetism, *Rev. Mod. Phys.*, vol. 25, pp. 233–238, Jan. 1953.
- [36] J. C. Slater, Ferromagnetism and the band theory, *Rev. Mod. Phys.*, vol. 25, pp. 199–210, Jan. 1953.
- [37] W. F. Brown, Jr., Theory of the approach to magnetic saturation, *Phys. Rev.*, vol. 58, pp. 736–743, 1940.
- [38] T. L. Gilbert and J. M. Kelly, Anomalous rotational damping in ferromagnetic sheets, in *Conf. Magnetism and Magnetic Materials*, Pittsburgh, PA, June 14–16, 1955. New York: American Institute of Electrical Engineers, Oct. 1955, pp. 253–263.
- [39] E. Della Torre and J. Eicke, *IEEE Trans. Magn.* 33, pp. 1251–154, 1997.

- [40] G. M. Sandler and H. N. Bertram, *J. Appl. Phys.* 81, pp. 4513–4515, 1997.
- [41] A. Kalimov, S. Vaznov, and T. Voronina, *IEEE Trans. Magn.* 33, pp. 1326, 1997.
- [42] C. Serpico, I. D. Mayergoyz, and G. Bertotti, *IEEE Trans. Magn.* 37, pp. 3546, 2001.
- [43] H. Ammari, A. Buffa, and J.C. Nedelec, A Justification of eddy currents for the Maxwell equations, *SIAM J. Appl. Math.*, 60(5), pp. 1805–1823, 2000
- [44] G. Bertotti, *Hysteresis in Magnetism*,. New York: Academic 1998, pp. 91–102
- [45] T.R. Koehler, Hybrid FEM-BEM method for fast Micromagnetic Simulations, *Physica B*, vol. 233, pp. 302–307, 1997
- [46] P.N. Brown, A.C. Hindmarsh, and L.R. Petzold, *SIAM J. Sci. Comput.*(USA) 15, pp. 1467–??, 1994
- [47] P.N. Brown, A.C. Hindmarsh, and L.R. Petzold Using Krylov Methods in the Solution of Large-Scale Differential-Algebraic Systems, *SIAM J. Sci. Comput.*, 15, pp. 1467–1488, 1994
- [48] P.N. Brown, A.C. Hindmarsh, and L.R. Petzold, Consistent Initial Condition Calculation for Differential-Algebraic Systems, *SIAM J. Sci. Comput.*, 19, pp. 1495–1512, 1998
- [49] Y. Saad and M.H. Schultz, GMRES: A Generalized Minimal Residual Algorithm for Solving Nonsymmetric Linear Systems, *SIAM J. Sci. Stat. Comp.* 7, pp. 856–869, 1986
- [50] I. D. Mayergoyz, C. Serpico, and Y. Shimizu, Coupling between Eddy Currents and Landau–Lifshitz dynamics, *J. Appl. Phys.*, vol. 81, no. 9, pp. 4513–4515, 2000

- [51] L. Torres, L. Lopez-Diaz, E. Martinez, and O. Alejo, Micromagnetic Dynamic Computations Including Eddy Currents, *IEEE Trans. On Magn.*, vol. 39, no5. , pp. 2498–2500, 2003
- [52] D. Suess, V. Tsiantos, T. Schrefl, J. Fidler, W. Scholz, H. Forster, R. Dittrich, J. Miles, Time resolved micromagnetics using a preconditioned finite element, *J. Magn. Magn. Mater.* 248, pp. 298–311, 2002.
- [53] R. Kikuchi, On the Minimum of Magnetization Reversal Time, *J. Appl. Phys.*, vol. 27, no. 11, pp. 1352–1357, 1956
- [54] L.Torres, E.Martinez, L. Lopez-Diaz, O. Alejos, About the inclusion of eddy currents in micromagnetic computations, *Physica B* 343,pp. 257–261, 2004
- [55] G. Albuquerque, J. Miltat, and A. Thiaville, Self-consistency based control scheme for magnetization dynamics, *J. Appl. Phys.*, Vol. 89, No. 11, pp. 6719–6721, 2001
- [56] A. Aharoni, Curling reversal mode in nonellipsoidal ferromagnetic particles, *J. Appl. Phys.*, Vol. 86, No. 2, pp. 1041–1046, 1999.
- [57] E.H. Frei, S. Shtrikman, And D. Treves, Critical Size and Nucleation Field of Ideal Ferromagnetic Particles, *Phys. Rev.*, Vol. 106, No. 3, pp.446–455, 1957.
- [58] S. Chikazumi, *Physics of Ferromagnetism*, Oxford University Press 1995
- [59] W. Rave, K. Fabian, A. Hubert, Magnetic states of small cubic particles with uniaxial anisotropy, *J. Magn. Magn. Mat.*, Vol. 190, pp. 332–348, 1998
- [60] M.E. Schabes, H. N. Betram, Magnetization processes in ferromagnetic cubes, *J Appl Phys* 64, pp 1347–1357, 1988

- [61] I. D. Mayergoyz, C. Serpico, and Y. Shimizu, J. Appl. Phys., Coupling between Eddy Currents and Landau-Lifshitz dynamics, vol. 81, no. 9, pp. 4513–4515, 2000
- [62] L. Torres, L. Lopez-Diaz, E. Martinez, and O. Alejo, Micromagnetic Dynamic Computations Including Eddy Currents, IEEE Trans. On Magn., vol. 39, no5., pp. 2498–2500, 2003
- [63] G. Albuquerque, J. Miltat, and A. Thiaville, Self-consistency based control scheme for magnetization dynamics, J. Appl. Phys., Vol. 89, No. 11, pp. 6719–6721, 2001
- [64] W. F. Brown, Jr., Micromagnetics (Krieger, Huntington, New York, 1978).
- [65] G. Hrkac, T. Schrefl, O. Ertl, D. Suess, M. Kirschner, F. Dorfbauer, J. Fidler, Influence of Eddy Current on Magnetization Processes in Sub-Micron Permalloy Structures, IEEE Trans. Magn., in press
- [66] D. R. Fredkin and T. R. Koehler, Hybrid Method for Computing Demagnetizing Fields, IEEE Trans. Magn. 26, pp. 415–417, 1990

Curriculum Vitæ

Dipl.-Ing. Gino Hrkac

Date of Birth January 20th 1976

Marriage Status unmarried

Nationality Austrian

Address Linzerstrasse 160/1/7
A-1140 Wien

Education 1982-1986 Elementary School, Vienna
 1986-1994 Scientific Grammar School, Vienna
 1994-1995 Military Service
 1998-2000 Studying Psychology at the University of Vienna
 1995-2003 Studying Physics at the Technical University of Vienna
 2002-2003 Master thesis with the IAEA
 June 2003 Graduated and achieved Master degree in Technical Physics
 since 2003 Institute of Solid State Physics, Technical University of Vienna PhD, Student

 Aug 2002-Oct 2002 Project at the International Atomic Energy Agency (IAEA) on NaJ (TI) and BGO detectors

 Oct 2002-July 2003 U and Pu Measurements for a Spectra Catalogue IAEA Research Contract No 10265/R0

 March 2005-Sept 2005 Research visit at the University of Sheffield, Sheffield, UK
 Aug 2005 Research visit at Hitachi San Jose Research Center

Lebenslauf

Dipl.-Ing. Gino Hrkac

Geboren am 20. Jänner 1976

Familienstand Ledig

Staatsbürgerschaft Österreich

Adresse, Linzerstrasse 160/1/7
A-1140 Wien

Ausbildung 1982-1986 Volksschule
1986-1994 Bundes Real Gymnasium (BRG 3)
1994-1995 Bundesheer
1998-2000 Studium der Psychologie and der Universität Wien
1995-2003 Studium der Technischen Physik an der TU-Wien
2002-2003 Diplomarbeit an der International Atom Energie Behörde (IAEA)
Juni 2003 Diplom in Technischer Physik
seit 2003 Wissenschaftlicher Mitarbeiter in der Arbeitsgruppe von T. Schrefl und J. Fidler.
Doktoratsstudium an der Technischen Universitt Wien
Aug 2002-Okt 2002 Projekt an der International Atom Energie Behörde (IAEA) mit NaJ (Tl) und BGO Detektoren
Okt 2002-Juli 2003 U und Pu Messungen für einen Spektrum Katalog IAEA Research Contract No 10265/R0
März-Sept 2005 Forschungsaufenthalt an der Universität von Sheffield, Sheffield, UK
Aug 2005 Forschungsaufenthalt bei Hitachi San Jose Research Center

List of publications

Journals and conference proceedings

1. G. Hrkac, T. Schrefl, O. Ertl, D. Suess, M. Kirschner, F. Dorfbauer, J. Fidler, "Influence of Eddy Current on Magnetization Processes in Sub-Micron Permalloy Structure", IEEE Trans. Mag., (2005), in press
2. G. Hrkac, M. Kirschner, F. Dorfbauer, D. Suess, O. Ertl, J. Fidler, and T. Schrefl, "Three-dimensional micromagnetic finite element simulations including eddy currents", G. Hrkac, M. Kirschner, F. Dorfbauer, D. Suess, O. Ertl, J. Fidler, and T. Schrefl, J. Appl. Phys. 97, 10E311 (2005).
3. M. Kirschner, T. Schrefl, G. Hrkac, F. Dorfbauer, D. Suess, J. Fidler, "Relaxation times and cell size in nonzero-temperature micromagnetics", Physica B, (2005), in press
4. D. Suess, T. Schrefl, R. Dittrich, M. Kirschner, F. Dorfbauer, G. Hrkac and J. Fidler, "Exchange spring recording media for areal densities up to 10 Tbit/in²", J. Magn. Magn. Mater. 290-291, 551-554, (2005).
5. M. Kirschner, T. Schrefl, F. Dorfbauer, G. Hrkac, D. Suess, and J. Fidler, "Three-dimensional micromagnetic finite element simulations including eddy currents", J. Appl. Phys. 97, 10E301 (2005).
6. T. Schrefl, M. E. Schabes, D. Suess, O. Ertl, M. Kirschner, F. Dorfbauer, G. Hrkac and J. Fidler, "Partitioning of the Perpendicular Write Field into Head and SUL Contributions", IEEE Trans. Magn., (2005)in press

7. R. Dittrich, T. Schrefl, M. Kirschner, D. Suess, G. Hrkac, F. Dorfbauer, O. Ertl, J. Fidler, "Thermally Induced Vortex Nucleation in Permalloy Elements", IEEE Trans. Mag., (2005), in press
8. D. Suess, T. Schrefl, M. Kirschner, G. Hrkac, J. Fidler, "Optimization of exchange spring perpendicular recording media", IEEE Trans. Magn., (2005) in press
9. D. Suess, T. Schrefl, S. Fahler, M. Kirschner, G. Hrkac, F. Dorfbauer, J. Fidler, "Exchange spring media for perpendicular recording, Appl. Phys. Lett., (2005) in press
10. F. Dorfbauer, T. Schrefl, D. Suess, M. Kirschner, G. Hrkac and J. Fidler, "Pulsed Inductive Microwave Magnetometer Response Calculated for IrMn/FeNi Bilayers", Europ. Phys. J. B, in press, (2004).
11. T. Schrefl, G. Hrkac, D. Suess, W. Scholz, and J. Fidler, "Coercivity and remanence in self-assembled FePt nanoparticle arrays", J. Appl. Phys. 93, 7041-7043, 2003

Books and book chapters

1. T. Schrefl, D. Suess, G. Hrkac, M. Kirschner, O. Ertl, R. Dittrich, and J. Fidler, "Nanomagnetism" in Advanced Magnetic Nanostructures, D Sellmyer, R Skomski (Eds), Springer, in press

Talks and conference contributions Invited lectures and talks

1. G. Hrkac, Influence of Eddy Current on Magnetization Processes in Sub-Micron Permalloy Structure, Department of Engineering Materials, University of Sheffield, United Kingdom, June 9, 2000

Contributed conference presentations

1. G. Hrkac, T. Schrefl, M. Kirschner, F. Dorfbauer, D. Suess, 3D Micromagnetic Finite Element Simulations Including Eddy currents, 49th Annual Conference on Magnetism and Magnetic Materials, Jacksonville/Florida, November 7-11, 2004.
2. D. Suess, M. Albrecht, T. Schrefl, R. Dittrich, M. Kirschner, F. Dorfbauer, G. Hrkac, J. Fidler, Exchange Spring Multilayer Media for High Density Recording, 49th Annual Conference on Magnetism and Magnetic Materials, Jacksonville/Florida, November 7-11, 2004.
3. R. Dittrich, T. Schrefl, D. Suess, M. Kirschner, F. Dorfbauer, G. Hrkac, J. Fidler, Optimization of MRAM switching by local variation of the Gilbert damping constant, 49th Annual Conference on Magnetism and Magnetic Materials, Jacksonville/Florida, November 7-11, 2004.
4. T. Schrefl, M. E. Schabes, D. Suess, O. Ertl, M. Kirschner, F. Dorfbauer, G. Hrkac and J. Fidler, Partitioning of the Perpendicular Write Field into Head and SUL Contributions, Intermag Conference 2005, Nagoya, Japan, April 2005.
5. R. Dittrich, T. Schrefl, M. Kirschner, D. Suess, G. Hrkac, F. Dorfbauer, O. Ertl, J. Fidler, Thermally Induced Vortex Nucleation in Permalloy Elements, Intermag Conference 2005, Nagoya, Japan, April 2005.
6. G. Hrkac, T. Schrefl, O. Ertl, D. Suess, M. Kirschner, F. Dorfbauer, J. Fidler, Influence of Eddy Current on Magnetization Processes in Sub-Micron Permalloy Structure, Intermag Conference 2005, Nagoya, Japan, April 2005.
7. D. Suess, T. Schrefl, M. Kirschner, G. Hrkac, J. Fidler, Optimization of exchange spring perpendicular recording media, Intermag Conference 2005, Nagoya, Japan, April 2005.
8. M. Kirschner, T. Schrefl, G. Hrkac, F. Dorfbauer, D. Suess, J. Fidler, Relaxation times and cell size in non-zero-temperature micromagnetics, 5th International Symposium on Hysteresis, Budapest, May, 2005

Poster presentations

1. G. Hrkac, M. Kirschner, T. Schrefl, F. Dorfbauer, D. Suess, J. Fidler, Micro-magnetic Simulations and Eddy-Currents Ultrabias, Summer School 2004, Anglet/France, September 12-16, 2004. (poster)
2. M. Kirschner, F. Dorfbauer, G. Hrkac, O. Ertl, P. Speckmayr, T. Schrefl, D. Suess, Vom Magnetkompass zum Terrabitspeicher - Simulation magnetischer Datenspeicherung, Scienceweek, Wien, 8.-16. Mai 2004. (poster)
3. D. Suess, T. Schrefl, R. Dittrich, M. Kirschner, F. Dorfbauer, G. Hrkac, Exchange spring recording media for areal densities up to 10 Tbit/in, JEMS04, Dresden, Germany, September, 2004. (poster)
4. M. Kirschner, T. Schrefl, F. Dorfbauer, G. Hrkac, D. Suess, J. Fidler, Cell size dependencies in non-zero temperature micromagnetics, Ultrabias Summer School 2004, Anglet/France, September 12-16, 2004. (poster)
5. M. Kirschner, T. Schrefl, F. Dorfbauer, G. Hrkac, D. Suess, J. Fidler, Cell Size Dependencies of Relaxation Times in Nonzero-temperature Micromagnetics, Nanomagnetism and Spintronics - Spring School, Cargese, Corsica, June 2005. (poster)
6. F. Dorfbauer, M. Kirschner, T. Schrefl, D. Suess, G. Hrkac, O. Ertl, J. Fidler, Analysis of Partially Disordered Nanoparticles, Nanomagnetism and Spintronics - Spring School, Cargese, Corsica, June 2005. (poster)